

Response to reviewers for the paper “Thermal dissociation cavity ring-down spectrometer (TD-CRDS) for the detection of organic nitrates in the gas and particle phase,” N.I.Keehan, et al.

We thank the reviewers for their comments on our paper. To guide the review process we have copied the reviewer comments in black text. Our responses are in **regular blue font**. We have responded to all the referee comments and made alterations to our paper (these are shown in **bold text**).

Anonymous Referee #1

Overview

The manuscript presents a TD-CRDS by coupling with a denuder to measure NO₂, peroxy nitrates (PNs), alkyl nitrates (ANs), and HNO₃ in the gas and particle phase. These mentioned NO_y species are pyrolyzed under their corresponding temperature windows and produce NO₂. NO₂ was then measured by a single commercial cavity ringdown NO₂ detector. They showed a feasible way to measure these species in chamber and field studies. They characterized the interference of N₂O₅ under high oxidants condition, and also assessed the interference of the recombination reaction by a model study. This work is valuable, but some comments should be addressed before publication

Major comments

R1.1. This work presented the results of the field measurement, but the interference caused by NO in the measurement system had not been considered. The related problems have been studied systematically in the article by Crowley group (e.g., Thieser et al., AMT, 2016; Sobanski et al., AMT, 2016). To make sense, this issue should be discussed.

Ref Thieser, J., Schuster, G., Schuladen, J., Phillips, G. J., Reiffs, A., Parchatka, U., Pohler, D., Lelieveld, J., and Crowley, J. N.: A two-channel thermal dissociation cavity ringdown spectrometer for the detection of ambient NO₂, RO₂NO₂ and RONO₂, *Atmos Meas Tech*, 9, 553-576, 10.5194/amt-9-553-2016, 2016.

Thank you for pointing this out. We have added the below text in section 3.7 discussing this consideration and referencing Thieser et al.

“In addition to the potential reduction in PNs signal due to recombination reactions, there is the potential for a spurious overestimation of PNs signal due to reactions of thermally dissociated peroxy or peroxy acetyl radicals with ambient NO in the presence of O₂, producing additional NO₂ (Thieser et al. 2016). This effect will be minimal in chamber simulations of nighttime chemistry, where the mixing ratio of NO is zero, but should be considered in any daytime field deployments.”

R1.2. Line 127-128, “a linear change,” is confused, which is not consistent with Eq. 2. For example, PNs equal to Oven3 minus Oven4, which means the NO₂ concentration is not

changed during the period of Oven3 and 4. In addition, the time resolution for a cycle is 8 minutes. On this time scale, the NO₂ concentration may change due to the emission. A parallel NO₂ measurement might be helpful in dynamic subtraction

We agree that the timescale of channel cycling is a substantial limitation of this instrument and concur with the reviewer's suggestion that a parallel NO₂ measurement could help in cases where NO₂ changes may be faster than changes in NO_y. We have revised the text as shown below to clarify the linear change assumption.

"Any concentration changes faster than the timescale of the channel cycle are accounted for by assuming a linear change in each channel between two consecutive samplings of that channel, and using the interpolated values at the timescale of the measuring channel for subtractions. This simplifying assumption only holds if the time between channel samplings is relatively short, and if there are no changes in background NO₂ on the timescale of the oven cycling. In situations where rapid NO₂ changes are likely, a parallel fast time resolution NO₂ measurement could be used to enable corrections for changing NO₂ background."

R1.3. Line 150, since the aerosol and gas-phase species have losses in the denuder and tube, and the aerosol result also affects the following subtraction of gas data, which means the corrections are necessary (the corrections are also important and not easy). The detailed corrections should be added in eq. 2 and well summarized in Sect. 3.9.

We have added a reference to the corrections discussion in Section 3.9 immediately before Eq. 2.

R1.4. How about the uncertainties of the measurement of these NO_y species?

Because the uncertainties of NO_y measurements are highly situationally dependent (e.g. is background NO₂ changing? What type of inlet is required in each experimental situation?), we feel these should be evaluated separately in each deployment of this instrument and do not feel it would be appropriate to assign a single value to them here.

R1.5. Before the heated gas and aerosol flowing into the CRDS, do you add a membrane to filter aerosol, if a membrane used, how about the frequency of the filter change, does trapped aerosol have the influence of on the measurement?

The commercial LGR CRDS instrument does have a teflon membrane filter on its inlet. In situations with high aerosol loading, this filter should be changed regularly to avoid the potential for any additional heterogeneous chemistry on collected aerosol. There is a pressure gauge in the ringdown cell that would provide a warning of a heavily loaded filter.

R1.6. I believe this system is more suitable for chamber study. According to the reported ANs

measurement in the previous literatures, the detection capacity of this instrument should be improved for better performance in the field measurement. Figure 9 also showed the ANs below the LOD (0.66 ppbv) in this field study.

We agree; in chamber studies experiments can be designed to avoid rapid background changes. We have added to the conclusions to underscore this: “This instrument has been successfully demonstrated for measurements on atmospheric simulation chambers operating at a wide range of concentrations and ambient measurements; **because of the increased uncertainty in the presence of rapid background changes in NO₂ mixing ratio, the TD-CRDS is best suited to chamber studies.**”

Technical corrections

R1.7. The temperature of the PNs measured in this article is only 130+273 K, is it possible due to the standard samples used in this work is much different with the standard samples applied in previous references, or the measured temperature is not equal to the real temperature in the oven?

Yes, it is true that the nominal oven temperature and the ‘real’ temperature inside the gas flow are not the same (see section 3.3). Complete dissociation was experimentally determined based on chamber generated Δ-carene peroxy nitrates.

R1.8. Line 78, delete the redundant “Nitrogen”

We thank the reviewer. The redundant “Nitrogen” has been deleted.

R1.9. Line 141, how about the time resolution of CRDS-NO₂, 1 s, 5 s or 10 s? please clarify it in the manuscript.

The time resolution of the CRDS-NO₂ is 1 s. The manuscript has been changed to add the following text:

“Since the CRDS-NO₂ takes a measurement every 1 sec, the last three measured points represent 3 seconds of sampling time”

R1.10. Line 161, “the interference of organic nitrates in the chemiluminescent measurement,” you mean the organic nitrates have the interference of NO₂ measurement in CL detector?

Yes. See Section 1 where we talk about CL interference due to the molybdenum catalyst. (Wooldridge et al. 2010)

R1.11. Line 284-285 Knopf et al., 2015 missed in the reference list

Thank you, re-added. (Knopf, Pöschl, and Shiraiwa 2015)

R1.12. Line 251, "Error is the standard deviation.", no errors listed here. The column format is not uniform in Table 2

Table 2 and accompanying table caption have been replaced with the following for clarity:

Table 2. Transmission of denuder at three concentrations of isobutyl nitrate (IBN) and one concentration of chamber-generated AN. Transmission is defined as the percentage of gas-phase alkyl nitrate that was passed through the denuder. Errors for 2016 measurements are the standard deviation.

Year	AN Source	Concentration (ppb)	Transmission through Channel 2 (385°C)
2016	IBN	250	(13.2±0.3) %
2016	IBN	385	(11.0±0.4) %
2016	IBN	800	(12.8±0.2) %
2019	d-carene	35	11.0 %

Table 1 formatting has been changed to match Table 2, along with clarifying text:

Table 1. Effect of inserting a single channel activated carbon denuder in between an NO₂ source and the TD-CRDS. Errors for the 2016 measurements are the standard deviation.

Year	[NO2] (ppb)	NO2 denuder transmission
2016	26	(3.3±0.3) %
2016	46	(3.1±0.2) %
2016	271	(1.96±0.08) %
2019	275	7.7 %

R1.13. Line 268, how long is the zero regular interval in general?

The following clarifying text has been added to the manuscript:

“The instrument is typically set to run its 3 minute zero every two hours.”

R1.14. Figure S4, since the linear model labeled as dash line, this figure needs to revise.

Thank you, we have updated the figure.

R1.15. Table S1 C3H70 correct to C3H7O

Updated.

R1.16. Figure S5, “left” and “right” in the caption correct to “top” and “bottom”

Updated, thank you!

Anonymous Referee #2

Keehan et al. describe the adaptation of a commercial CRDS NO₂ instrument for measuring classes of thermally labile nitrates in both the gas and particulate phases. The thermal-decomposition technique for measuring classes of nitrate compounds has been an important tool for constraining concentrations of unknown nitrate species and e.g. NO_x / NO_y budget closure studies. Typically, these types of measurements have been demonstrated using custom-built NO₂ sensors, and it is therefore quite useful to show that a commercial NO₂ sensor can also be used to produce sufficient data quality for e.g. laboratory and urban studies. The paper is well written and thorough and I think deserves publication in AMT after addressing some suggestions and questions that I outline below. I do think there are some important issues that the authors should address in the revision. These are listed in the specific comments below but I will reiterate them here: 1) Why is the inlet transmission of N₂O₅ believed to be so low and how do we know that the inlet transmission for other species, e.g. HNO₃ or AN, is not also low? NO₂ and particulate RONO₂ are somewhat validated by comparison to other instruments, but I do not believe that absolute standards of other species are presented. 2) Please carefully check figure 5 and the discussion surrounding the thermal decomposition of N₂O₅ and NO₃, as discussed below. 3) How could a pressure reduction upstream of the heaters change the recombination of thermally decomposed species?

General comments

R2.1) Line 23: I'm not sure why the word “oxidized” is here

This was to indicate that some of the VOCs might already be oxidized, but this is not an essential point. Since it may be confusing, we've removed it.

R2.2) Line 65-67: Molybdenum catalysts are also widely recognized to convert some other NO_y species, not just NO₂, into NO, which would cause a significant problem for this work.

Precisely this is the benefit of the use of CRDS detection of NO₂, rather than chemiluminescence with Mo catalyst, in this work.

R2.3) Line 67-68: I would say for LIF the limit is laser power not cavity length. A Multipass cell essentially increases laser power in the middle of the cell.

We have updated the text to replace the reference to cavity length with laser power.

R2.4) Line 78: remove first word

Done, thank you (see R1.8).

R2.5) 102-104: I was confused by mentioning LGR CRDS with two flow rates. Recommend clarifying that the two are different instruments and that the second one is for the present work.

Different flow rates between our instrument and the instrument described in Paul et al required that for equal residence times, we needed a different length oven. To clarify, we removed "LGR" in front of the CRDS in line 103.

"A length of 55 cm was calculated from Equation 1 using the Paul et al. CRDS flow rate (q = 2.5 lpm) and oven length (h= 64 cm) in order to give our instrument equal residence times (τ , see Eq. 1). Since the flow rate of the LGR CRDS is significantly smaller (1.2 lpm), the required tube length is shorter than that reported in Paul et al."

R2.6) 106: Metric units please

The nominal part name was chosen to represent the industry standard size "1/4", not a measurement. For clarity the manuscript has been changed to the following:

"These ovens were attached to nominal 1/4 inch (0.635 cm) Teflon tubing with Teflon Swagelok tees and unions. Teflon connectors were chosen over stainless steel to reduce destruction of NO₂ by heated steel (Hargrove and Zhang 2008). An oven-length piece of 1/4 inch (0.635 cm) Teflon is used as the ambient temperature background NO₂ channel, which has a typical temperature of 22 - 24° C inside the inlet box. [...] The denuder is a 45 cm long cylinder of activated charcoal with a 1/4 inch (0.635 cm) channel through the center."

R2.7) 135: It seems likely the settling time might be significantly reduced by maintaining flow through all channels at all times. Recommend the authors consider this for future deployments, or comment in the manuscript if they know that this would not help.

The following text was added to section 2 to address the possibility of a continuous flow setup:

“(We note that maintaining a constant flow through each of the channels at all times would help to reduce the stabilization time in the CRDS, leading to a reduced time resolution. Because the CRDS has its own internal pump to draw air into the CRDS cell, a secondary pump would be required to maintain constant air flow through the non-sampling channels. Such a modification could help make this instrument more viable for high time resolution ambient measurements.)”

R2.8) 145: Is there ever any aerosol NO₂ detected or could this sampling mode be eliminated?

We have found “NO₂ aerosol mode” useful in diagnosing instrument contamination problems, interferences not yet accounted for, and false values caused by rapid changes to an unstable system. It isn’t totally necessary, but it can be valuable for data analysis post-experiment. We sometimes see signal in the “NO₂ aerosol” channel, but it is usually indicative of other instrument issues, not “real” NO₂ aerosol.

The following addition was made to the manuscript:

“While there is not expected to be any signal in the NO₂ aerosol channel, the channel has proven useful for diagnosing contamination problems, interferences not yet accounted for, and false values caused by rapid changes.”

R2.9) Section 3.1: Can you say a bit more about how the comparison with the commercial NO_x sensor was performed? Was this performed over a short time period by dynamically diluting air from the lab which is expected to be a relatively constant mixture during the experiment? If so, any interference would not be a constant offset but would scale with the dilution. I am actually surprised that the slope is so close to 1, as I expected that the molybdenum converter converted many NO_y species. Conversion of Nitric acid seems like another likely positive interference with the CL instrument. It may be that that sensor reports 0.64 ppb even when sampling clean zero air due to a background from the converter. How is the zero for the CRDS determined? Is the laser tuned off of an NO₂ resonance or is a periodic zero air sampling period required?

Yes. This was performed using dilutions of lab air in zero air over a short period of time. The fact that the slope is so close to 1 is likely due to ambient concentrations of NO_y being low compared to NO₂, explaining why the interference does not significantly scale with dilution. The urban location of the lab would support the relatively low levels of NO_y compared to NO₂. The 4% difference in slope could be from dilution effects of the NO_y being detected as NO₂.

We agree that a converter background could account for some or all of the zero offset in the Thermo chemiluminescence instrument. That’s why this instrument is not designed around a Thermo CL.

The LGR has an internal NO₂ scrubber that it uses to generate zero air for the zero measurement, described on line 280.

The text has been amended:

“Since this experiment was performed using dilutions of zero air, any interference from NOy species in the CL detector would also be expected to scale with dilution. The urban location of the lab would support the relatively low levels of NOy compared to NO2, explaining the very small 4% difference in slope between the two detectors.“

and

“The intercept offset of the low concentration experiment is 0.64 ppb, which may be attributable to the interference of organic nitrates in the chemiluminescence measurement, or a slight zero offset in the chemiluminescence detector”

R2.10) 174: In my experience, the certification on those cylinders is not good for more than 1 year and significant loss of NO2 in the cylinders is sometimes observed over longer periods. Perhaps this one is different.

True, this is an older cylinder, but it's the only one we had available. This concern is valid.

R2.11) Line 188: “delta-3-carene”

The line was corrected to read:

“NO3 + Δ-3-carene mixture”

R2.12) Section 3.3 / Figure 4: How is it known that the observed thermogram from ~50 – 100C (PNs) is from peroxy nitrates and not from N2O5? Can the authors cite a paper showing that the formation of peroxy nitrates are expected from the reaction of D-3- carene + NO3?

The concentration of reactants is chosen such that all NO₃, and hence N₂O₅, is consumed in this experiment. Further empirical evidence of the lack of N₂O₅ is that it does not plateau at 130 C, as do PN (see figure 5). Unlike ANs and PN that dissociate in a plateau at a specific temperature, N2O5 seems to partially dissociate over a large range of temperatures. (see also Womack et al 2017)

R2.13) Section 3.4 / Figure 5: I am confused by this figure. The gray line shows much more noise than the black, and when I first looked at it assumed the gray line was for the low oxidant experiment although now see that the caption suggests otherwise.

The precision shown on the black line against the left axis seems better than is expected for the stated detection limit of the CRDS instrument. So – can the authors please check that the legend and axes are labeled properly? If they are reversed this would change some of the discussion.

The legend is accurate. Likely the noise of the high oxidant experiment is very large because we were approaching the upper limits of the CRDS, where ringdown times are so rapid that their fit is more poorly defined, resulting in an increase in noise.

Also, for the low oxidant experiment, as shown on the left axis, the thermogram shows a > 5 ppb range of NO₂, while the caption says that 3.2 ppb was used. Could the authors provide a bit of discussion here surrounding what is expected from the experiment, e.g. is it expected that in the low oxidant experiment all of the NO₂ would be lost to the NO₃ + alkene reaction by the time the air is sampled by the instrument, and so we should expect to see about as much RONO₂ as there was initially NO₂?

The 3.2 ppb was an estimate from the lowest possible NO₂ concentration possible from our 514 ppm NO₂ cylinder calculated by flow rate, by dilution in zero air. The mixing ratio listed is thus spuriously precise, and there is likely some zero offset, which we do not routinely correct for in thermograms. To avoid confusion, we change the reported NO₂ mixing ratio to be clearer about how it is an approximate amount (~ 3 ppb instead of 3.2 ppb).

I was somewhat confused by the discussion surrounding the appearance of N₂O₅ in the thermograms. Initially I thought that the authors were suggesting that N₂O₅ \rightarrow NO₃ + NO₂ was resulting in the increase in signal > 200 C, but later realized they were talking about NO₃ \rightarrow NO₂ + O. I suggest this section starts with a brief discussion of the two-step thermal decomposition of N₂O₅, and I would not refer to NO₃ \rightarrow NO₂ + O as thermal dissociation of N₂O₅. Could the authors indicate where N₂O₅ \rightarrow NO₃ + NO₂ is visible in the thermogram? Also, what effect is there from thermal decomposition of O₃ followed by NO₃ + O \rightarrow NO₂ + O₂?

N₂O₅ to NO₂ and NO₃ is not a nice plateau on the thermogram, thus the problem. This first dissociation step seems to occur split across the PN and AN ovens. The second dissociation step (NO₃ \rightarrow NO₂ + O) may also contribute in the ANs channel, and the rest in the HNO₃ channel. The suggestion to clarify this at the beginning of this section is good; we added earlier reference to reactions R3 & R4

I am quite surprised by the very low transmission / detection of N₂O₅ in the system, as I would not have thought based on the previous similar studies that N₂O₅ was much more difficult to sample than the other classes of nitrates. The stated detections in the PN and AN channels (7% and 28%) are difficult to reconcile. If N₂O₅ is completely dissociated in the PN channel, and the conclusion is that only 7% of N₂O₅ must be transmitted through the inlet, than I would expect at most another 7% of signal from the NO₃ decomposition (total of 14% instead of 28%). But still, in the AN channel only a fraction of NO₃ is dissociated. Did I miss something here? Is there another study that could be cited that reports low transmission of N₂O₅ through Teflon tubing?

Inlet transmission is only part of the problem, dissociation of N₂O₅ spread across multiple temperatures also complicates detection. We interpret this as arising because the

recombination to N₂O₅ is rapid, and thus some NO₂ remains bound up in this reservoir until very high temperatures. The first dissociation does not occur to completion in the PNs channel, so the lower percentage there (7%) does not mean only another 7% would dissociate. In fact, it seems that the 7% and 28% are both mainly the first dissociation of N₂O₅, with the second dissociation (NO₃) occurring only at the highest temperature oven.

This text was added to section 3.4 to clarify this: “We note that due to its high reactivity and wall losses (especially the NO₃ fragment), **as well as the likelihood that some N₂O₅ remained incompletely dissociated even at the ANs oven temperature**, the total N₂O₅ detection is substantially less than 100% of the N₂O₅ concentration present in the chamber. **We also emphasize that these percentages are specific to the configuration used in this characterization experiment: from the chamber containing the modeled N₂O₅ concentration used to determine these interference percentages, a 2-m Teflon inlet line led to the TD-CRDS instrument.**”

R2.14) Section 3.7 / 3.8: The dependence of the inlet heater conversion efficiency and chemistry on the pressure within the heater is not discussed, but may be worth consideration for the authors in the future. My expectation is that if a lower pressure is used within the heater, this would greatly reduce the recombination. Perhaps it is not used that way here because this would require lower pressure within the CRDS and possibly lower precision. If so, it is a worthwhile point of discussion when considering differences between CRDS and LIF detection of NO₂.

We agree that lower pressure would absolutely help reduce recombination, but would not be possible using this commercial LGR CRDS back end. We added a mention of the advantage of lower cell pressure to reduce recombination to the discussion of comparison to LIF in the introduction:

“LIF can be tuned to a specific spectroscopic transition like CRDS, **and can be run at lower cell pressures that reduce recombination (see section 3.7 below), but ...**”

R2.15) Line 284: please include the Knopf et al citation in the Reference list.

Thank you, added, see R1.11.

Also, I presume that the OH loss rate was calculated based on the uptake coefficient stated in that paper using the conditions for this experiment. If so, I suggest the authors state that here because as it is it sounds like the 46 / s number came directly from that paper.

Text was changed to read:

“**[...] and OH wall loss rate (calculated to be 46 s-1 for these conditions) from Knopf, Pöschl, and Shiraiwa 2015.**”

R2.16) Section 4.1: Were any particulate peroxy nitrates detected using the TD-CRDS instrument? Is it known how those would be classified by AMS?

We did not operate at conditions that produced substantial peroxy nitrates for this comparison, and we do not know if these would also appear as pRONO₂ to the AMS.

Thermal dissociation cavity ring-down spectrometer (TD-CRDS) for detection of organic nitrates in gas and particle phase

Natalie I. Keehan,¹ Bellamy Brownwood,¹ Andrey Marsavin,¹ Douglas A. Day,² and Julianne L. Fry^{1,*}

⁵ Chemistry Department and Environmental Studies Program, Reed College, Portland, OR 97205, USA

² Cooperative Institute for Research in Environmental Sciences (CIRES) and Department of Chemistry, University of Colorado, Boulder, CO 80303, USA

Correspondence to: J. L. Fry (fry@reed.edu)

10

Abstract. A thermal dissociation – cavity ring-down spectrometer (TD-CRDS) was built to measure NO₂, peroxy nitrates (PNs), alkyl nitrates (ANs), and HNO₃ in the gas and particle phase. The detection limit of the TD-CRDS is 0.66 ppb for ANs, PNs, and HNO₃ and 0.48 ppb for NO₂. For all four classes of NO_y, the time resolution for separate gas and particle measurements is 8 minutes and for total gas + particle measurements is 3 minutes. The accuracy of the TD-CRDS was tested by comparison of NO₂ measurements with a chemiluminescent NO_x monitor, and aerosol-phase ANs with an Aerosol Mass Spectrometer (AMS). N₂O₅ causes significant interference in the PNs and ANs channel under high oxidant concentration chamber conditions, and ozone pyrolysis causes a negative interference in the HNO₃ channel. Both interferences can be quantified and corrected for, but must be considered when using TD techniques for measurements of organic nitrates. This instrument has been successfully deployed for chamber measurements at widely varying concentrations, as well as ambient measurements of NO_y.

1 Introduction

Nitrogen oxide based functional groups are an area of significant interest in atmospheric oxidative chemistry. Organic nitrates are formed through reactions between volatile organic compounds (VOCs), of which the global majority are biogenic in origin (Seinfeld and Pankow 2003; Perring, Pusede, and Cohen 2013) and NO_x (=NO+NO₂) or NO₃ (Ng et al. 2017), which is predominantly anthropogenic in origin (Seinfeld and Pandis 2006). The two major organic nitrate products of these reactions are alkyl nitrates (ANs) of the form RONO₂ and peroxy nitrates (PNs) of the form ROONO₂. These organic nitrates play an important role in regulating ozone in the troposphere by serving as temporary reservoirs of NO₂ (Buhr et al. 1990; Thornton et al. 2002). Equilibrium partitioning of high molecular weight, low volatility organic molecules occurs, causing some organics to condense onto existing particles (Jimenez et al. 2009). These secondary organic aerosols (SOA) consist primarily of the highly oxidized products of VOC + oxidant reactions, because of their increased molecular weight and higher polarity. Lower night-time temperatures decrease volatility even further, leading to increased partitioning into the particle phase (Fry et al. 2013). Warmer temperatures, deposition, and chemistry within the particles change the equilibrium, resulting in the release of NO₂. Because of long residence times of SOA, significant quantities of NO₂ can be transported away from source regions by

Deleted: (oxidized)

35 wind in reservoir form ([Perring, Pusede, and Cohen 2013; Browne et al. 2013; Wolfe et al. 2007; Kim et al. 2014; Zare et al. 2018](#)).

Different classes of organic nitrates dissociate in distinct temperature ranges, based upon the inherent stability of the molecules. At residence times of 30-90 ms in quartz tubes, peroxy nitrates (PNs, RO_2NO_2) dissociate at approximately 150°C, alkyl nitrates (ANs, RONO_2) at 350°C, and nitric acid (HNO_3) at 600°C ([Day et al. 2002](#)). The dissociation temperatures are 40 dependent on residence times, but there seems to be very little dependence on what constitutes the R group ([Hao et al. 1994; Kirchner et al. 1999](#)). This is useful for the detection of total peroxy and alkyl nitrates (Σ PNs and Σ ANs, respectively) because they can be dissociated as a class, with identical detection efficiency regardless of the chemical nature of the R group. Reaction 1 shows that the thermal dissociation of each class of organic nitrates results in one NO_2 and a hydrocarbon-containing X group.



where $\text{X} = \text{RO}_2, \text{RC(O)OO}, \text{RO}, \text{or OH}.$

PNs serve as a temporary reservoir of NO_2 in the atmosphere, because the equilibrium between formation and dissociation is rapid. For example:



50 has a K_{eq} of $2.2 \times 10^{-12} \text{ cm}^3 \text{ molecules}^{-1}$, resulting in a PN lifetime at 20 ppb NO_2 of 0.56 seconds at 298K and 1 bar ([Atkinson et al. 2006; JPL Data Evaluation 2015](#)). In contrast, ANs and HNO_3 predominantly serve as sinks of NO_2 , with spatial transport scales that depend on their meteorology-dependent deposition lifetimes ([Horowitz et al. 2007](#)).

Previous studies of organic nitrates have been done by measuring specific nitrates ([Wolfe et al. 2007; Horowitz et al. 2007; Parrish and Fehsenfeld 2000; Surratt et al. 2006; Lee et al. 2016](#)) or by looking at the sum of nitrates using thermal dissociation

55 NO_2 measurements ([Zellweger et al. 1999; Day et al. 2002; Hargrove and Zhang 2008; Paul, Furgeson, and Osthoff 2009; Rollins et al. 2010; Sobanski et al. 2016](#)). The instrument described in this paper has drawn on aspects of three different thermal dissociation nitrate measurement strategies in the literature. The general oven and flow plan was based on the thermal dissociation-laser induced fluorescence (TD-LIF) instrument built by the Cohen group at UC Berkeley ([Day et al. 2002](#)). Instead of LIF, the NO_2 detection device in the instrument described here is a commercial cavity ring-down spectrometer 60 (CRDS). Once interferences are characterized and absorption cross-sections are known, CRDS does not require in-line calibration by an authentic standard gas cylinder during sample measurement, as discussed in Paul et al. ([Paul, Furgeson, and Osthoff 2009](#)). Gas-particle partitioning measurements using a switchable charcoal denuder was incorporated from Rollins et al. ([Rollins et al. 2010](#)).

The benefit of using CRDS over chemiluminescence (CL) detection of NO_2 is its selectivity. The (partial) thermal dissociation 65 of multiple unstable nitrate compounds like ANs, PNs, and N_2O_5 into NO_2 by the CL heating process and molybdenum catalyst has been well documented ([Wooldridge et al. 2010](#)). CRDS can make direct measurements of NO_2 , unlike CL, which uses a metal catalyst to turn NO_2 into NO and back-calculates NO_2 concentration by subtraction. CRDS does not require heating or a catalyst, and is therefore more selective. LIF can be tuned to a specific spectroscopic transition like CRDS, [and can be run](#)

at lower cell pressures that reduce recombination (see section 3.7 below), but laser power becomes limiting for measurement

70 of low concentrations, and requires delicately aligned multipass optical cells to achieve low limits of detection for NO₂. The downsides of CRDS come from the expense and delicateness of the instrument.

Since high molecular weight oxidation products can condense into the particle phase, it is valuable to be able to make both gas and particle phase measurements. Denuders work by using diffusion to separate gases from liquid- or solid-phase particles. Higher diffusion rates for gases means that they are more readily absorbed into the walls of a charcoal denuder, leaving behind 75 the particle phase. The fraction of gas removed depends on residence time in the denuder and the surface area available to diffusing gas molecules. The diffusion coefficient of NO₂ is reported to be 0.154 cm²s⁻¹ ([Williams et al. 2012](#)) and 0.070 cm²s⁻¹ for n-propyl nitrate ([Paul, Furgeson, and Osthoff 2009](#)). According to previous studies using charcoal denuders, the denuder removed the majority of particles with diameters <0.1 μm ([Glasius et al. 1999](#)) as well as all semivolatile organic gases.

Deleted: cavity length

2 Instrument design

80 In order to measure concentrations of organic nitrates by thermal dissociation, a multi-channel, switchable, controllable heating inlet system was constructed. This heating unit was then attached to a cavity ring-down NO₂ detector (CRDS, Los Gatos Research Inc. Model #907-0009) to complete the instrument. An overall instrument schematic is shown in Figure 1a.

Deleted: Nitrogen

The three quartz tube ovens were constructed out of 55 cm long, 3.8 mm inner diameter (ID), 7.0 mm outer diameter (OD) 85 quartz tube wrapped in 15 cm nichrome wire (2mm wide ribbon with resistivity of 11 Ω/m) located 5 cm from one end. An 18 cm long, 8 mm ID, 10 mm OD quartz tube was slipped around the nichrome section to hold it in place. Over the 8mm ID tubing, two 8 cm long, 10.5 mm ID, 13 mm OD quartz tubes were placed with a thermocouple in between to hold the end of the thermocouple in place. The whole heated section was wrapped in ½" thick ceramic insulation (McMaster-Carr # 9379K92) with foil coating, as shown in Figure 1b. It is important to note that the heat capacity of the oven is determined by the effectiveness of the insulation. Insufficient insulation can result in unstable oven temperatures or increase the time required 90 for the gas to reach the required dissociation temperature, leading to increased sampling times on each oven and a degradation of the time resolution of the instrument.

Deleted:) located

The thermocouple was placed so it was the same distance and glass thickness from the nichrome as the nichrome was from the gas flow, so it was hypothesized that the thermocouple temperature reading would be representative of the internal temperature of the oven. Experiments comparing this external thermocouple to a thermocouple placed at the same position inside the gas 95 flow showed that the average internal oven temperature was between 25 and 30°C hotter than the external thermocouple reading. Because of the oven design, the temperature inside the heated portion of the oven is not uniform, but is hottest closest to the end of the nichrome section, nearer to the exhaust.

The unheated portion of the quartz tubing used in this instrument is significantly shorter in length than the length originally calculated in Day et al. (2002) due to additional testing reported in Paul et al. (2009) ([Paul, Furgeson, and Osthoff 2009](#)). The 100 shorter length was chosen to suppress the recombination reaction of NO₂ radical with the organic sister product upon cooling.

The shorter ovens were shown to effectively reduce residence time, and therefore recombination, but still allowed adequate time for gas cooling before entering the sampling chamber. A length of 55 cm was calculated from Equation 1 using the Paul et al. CRDS flow rate (q = 2.5 lpm) and oven length (h= 64 cm) in order to give our instrument equal residence times (τ, see Eq. 1). Since the flow rate of the LGR CRDS is significantly smaller (1.2 lpm), the required tube length is shorter than that reported in Paul et al.

$$\tau = \frac{\pi r^2 h}{q} \quad (\text{Eq. 1})$$

110 These ovens were attached to nominal 1/4 inch (0.635 cm) Teflon tubing with Teflon Swagelok tees and unions. Teflon connectors were chosen over stainless steel to reduce destruction of NO₂ by heated steel (Hargrove and Zhang 2008). An oven-length piece of 1/4 inch (0.635 cm) Teflon is used as the ambient temperature background NO₂ channel, which has a typical temperature of 22 - 24° C inside the inlet box. The three ovens and background channel connect to a six-port solenoid valve with Teflon wetted surfaces. The outlet of the solenoid valve runs to the inlet of the LGR CRDS.

115 The inlet of the instrument has two possible pre-oven pathways: denuded and undenuded. The denuder is a 45 cm long cylinder of activated charcoal with a 1/4 inch (0.635 cm) channel through the center. A three-way, Teflon-wetted solenoid directs the inlet air either through the denuder or through an equivalent length of Teflon tubing before the air sample enters the ovens. An Omega CN616TC1 Temperature Controller was used to regulate the temperature of the ovens. The inlet end of the oven nichrome wire was attached to the positive terminal of the Mouser 24VDC power supply and the exhaust end was wired to a

120 Mouser DR06D12 solid state relay. These relays received signals from the temperature controller, either allowing or prohibiting current flow through the nichrome wire by completing the circuit loop. The temperature controller was able to detect the temperature of the ovens using K-type thermocouples. The desired temperatures were set using the CN616 Software provided with the temperature controller. Experiments showed that a single 24V power supply did not provide enough current to heat the Channel 1 oven to an appropriate temperature, so a second 24V power supply was used to supply power to Channel

125 1. This succeeded in getting the oven as high as 820°C; the typical temperature setpoint was 700°C.

Valve switching was controlled by a Measurement Computing (MCC) USB-ERB08 relay module. Each solenoid was soldered to a diode to prevent damage from voltage spikes generated by switching. These leads were then connected to the normally closed (NC) ports of the MCC relay unit, which completed the circuit to open the specified valve.

One limitation of the TDCRDS instrument is its reliance on a single detector. This necessitates sequential measurements of 130 each relevant species, creating a minimum time resolution for the instrument. This minimum time resolution can be large compared to the rate of change of the measured species in the atmosphere or in a chamber experiment. Any concentration changes faster than the timescale of the channel cycle are accounted for by assuming a linear change in each channel between two consecutive samplings of that channel, and using the interpolated values at the timescale of the measuring channel for subtractions. This simplifying assumption only holds if the time between channel samplings is relatively short, and if there are no changes in background NO₂ on the timescale of the oven cycling. In situations where rapid NO₂ changes are likely, a parallel fast time resolution NO₂ measurement could be used to enable corrections for changing NO₂ background. The goal is

Formatted: Font: (Default) Times New Roman, 10 pt, Not Bold, Font color: Auto, English (US)

Deleted: A length of 55 cm was calculated from Equation 1 using the flow rate determined by the LGR CRDS (q = 2.5 lpm) and length of the shorter oven (h = 64 cm) reported in Paul et al., in order to give our instrument equal residence times (τ, see Eq. 1). Since the flow rate of the LGR CRDS is significantly smaller (1.2 lpm), the required tube length is shorter. ¶

Deleted: 1/4"

Formatted: Font: (Default) Times New Roman, 10 pt, Not Bold, Font color: Auto, English (US)

Formatted: English (US)

Formatted: Font: (Default) Times New Roman, 10 pt, Not Bold, Font color: Auto, English (US)

Deleted: 1/4"

Formatted: Font: (Default) Times New Roman, 10 pt, Not Bold, Font color: Auto, English (US)

Deleted: 1/4"

Formatted: Font: Not Italic

Deleted: C

Formatted: Subscript

Formatted: Subscript

Formatted: Subscript

Formatted: Subscript

to minimize the instrument time resolution by minimizing the sampling time of each oven without introducing error caused by mixing analyte in the tubing between the switching valve and the CRDS sample cell. Plausible channel switching rates between 30 and 90 seconds were tested to measure the stabilization time of each channel. This testing was conducted by flowing 10 sccm of zero air through a three-necked round bottom flask containing 0.2 ml of isobutyl nitrate (IBN) chilled to -21°C. This 150 10 sccm flow was diluted with 7.25 lpm of zero air to achieve a concentration of ~ 700 ppb.

Figure S2 shows the NO₂ vs time curve for the TD-CRDS when gas was sampled with various lengths of time in each oven. The high concentration peaks are when the IBN dilution is flowing through Channels 1 and 2 (650°C and 385°C, respectively) and the troughs are IBN flowing through Channels 3 and 4 (120°C and ambient 23°C, respectively). For this application, 45-155 second channel time yielded the best trade-off between channel stabilization and time resolution. (We note that maintaining a constant flow through each of the channels at all times would help to reduce the stabilization time in the CRDS, leading to a reduced time resolution. Because the CRDS has its own internal pump to draw air into the CRDS cell, a secondary pump would be required to maintain constant air flow through the non-sampling channels. Such a modification could help make this instrument more viable for high time resolution ambient measurements.)

160 Channel timing with the denuder was determined in a similar manner, and it was determined that 1 minute per channel was necessary to achieve stabilization with the charcoal denuder. This leads to an 8 minute complete cycle time, since there is 1 minute for denuded and 1 minutes undenuded on each of the four species channels. The last 3 measured points in each channel period are averaged to obtain the concentrations that are used for each channel. Since the CRDS-NO₂ takes a measurement every 1 sec, the last three measured points represent 3 seconds of sampling time. A full cycle in this gas / aerosol mode is 165 shown in Figure 2.

For each full cycle of concentration measurements from the eight channels, the concentrations of the individual classes of NO_y are determined by subtractively as follows. Section 3.9 below discusses subsequent corrections that are applied to each channel.

$$\text{Total NO}_2 = [\text{NO}_2]_{\text{oven } 4} \quad \text{Aerosol NO}_2 = [\text{NO}_2]_{\text{oven } 4, \text{ denuded}} \quad (\text{Eqs. 2})$$

$$\text{Total PNs} = [\text{NO}_2]_{\text{oven } 3} - [\text{NO}_2]_{\text{oven } 4} \quad \text{Aerosol PNs} = [\text{NO}_2]_{\text{oven } 3, \text{ den}} - [\text{NO}_2]_{\text{oven } 4, \text{ den}}$$

$$170 \quad \text{Total ANs} = [\text{NO}_2]_{\text{oven } 2} - [\text{NO}_2]_{\text{oven } 3} \quad \text{Aerosol ANs} = [\text{NO}_2]_{\text{oven } 2, \text{ den}} - [\text{NO}_2]_{\text{oven } 3, \text{ den}}$$

$$\text{Total HNO}_3 = [\text{NO}_2]_{\text{oven } 1} - [\text{NO}_2]_{\text{oven } 2} \quad \text{Aerosol HNO}_3 = [\text{NO}_2]_{\text{oven } 1, \text{ den}} - [\text{NO}_2]_{\text{oven } 2, \text{ den}}$$

The "Total" concentrations in Eqs. 2 refer to gas + aerosol phase, to obtain gas-phase only concentrations, the aerosol can be subtracted from the total for each channel. While there is not expected to be any signal in the NO₂ aerosol channel, the channel has proven useful for diagnosing contamination problems, interferences not yet accounted for, and false values caused by rapid 175 changes to an unstable system.

Deleted: 1

Deleted: M

Deleted: Unfortunately, the use of a commercial CRDS limits the flexibility of the instrument setup. Since

Deleted: This secondary pump could not be placed at the inlet of the instrument, as a 'push' pump, in order to preserve aerosols for measurement. Placing a second 'pull' pump on the back end would greatly increase the internal tubing of the instrument, leading to increased time for recombination of the heat-dissociated NO₂ species. ...

Formatted: Subscript

Deleted: :

Formatted: Font: (Default) Times New Roman, 10 pt, Not Bold, Font color: Auto, English (US)

Formatted: Font: (Default) Times New Roman, 10 pt, Not Bold, Font color: Auto, English (US), Subscript

Formatted: Font: (Default) Times New Roman, 10 pt, Not Bold, Font color: Auto, English (US)

3 Calibration and characterization

3.1 Determination of NO₂ sensitivity

Two sets of tests were performed to verify the sensitivity of the LGR CRDS to NO₂. Response at high concentrations was verified at concentrations of 250 to 1000 ppb using dilutions of NO₂ in zero air. A 514.5 ppm calibrated mixture of NO₂ in N₂ (Airgas) was diluted with a zero air source to generate the required mixing ratios. Response at low concentrations was compared to a Thermo chemiluminescent NO_x detector between 1.5 to 11.5 ppb. Low concentration NO₂ was obtained using ambient lab air diluted using zero air. The results of these experiments are shown in Figure 3.

The fit line has a slope of close to 1 over both measured ranges, indicating good agreement under both high and low concentration conditions. ~~Since this experiment was performed using dilutions of zero air, any interference from NO_x species in the CL detector would also be expected to scale with dilution. The urban location of the lab would support the relatively low levels of NO_x compared to NO₂, explaining the very small 4% difference in slope between the two detectors.~~ These experiments suggest an upper limit error due to the NO₂ detection of 10%. The intercept offset of the low concentration experiment is 0.64 ppb, which may be attributable to the interference of organic nitrates in the chemiluminescence measurement, or a slight zero offset in the chemiluminescence detector. Thus, the CRDS is accurate under both atmospherically relevant and elevated laboratory experiment conditions, but regular calibration against a known source or comparison with another NO₂ measurement is nevertheless recommended.

3.2 Production of alkyl nitrates and peroxy nitrates using the Reed Environmental Chamber (REC) for TD-CRDS instrument characterization

The 400 L Teflon bag Reed Environmental Chamber ([REC, Draper et al. 2015](#)) was used to generate VOC + NO₃ reaction products that could be analyzed using the TD-CRDS. The REC chamber was operated with steady inlet flows to the top of the chamber of zero air (4.3 lpm), O₃ (200 sccm), NO₂ (4.4 sccm of 515 ppm), and VOC (14.2 sccm zero air through chilled liquid source containing gas-phase VOC of ~100 ppm), which mix and react (average residence time ~ 90 minutes) and are sampled for analysis from the bottom of the chamber. Zero air was generated using a Sabio Model 1001 zero air generator, which removes water, particulates, and reactive gases. Ozone was generated using a UV light source (Pen-Ray Hg lamp at 254 nm) inside the middle neck of a three-necked round bottom flask, and the concentration was altered by adjusting the depth of the light source in the flask. The constant NO₂ source was a gas cylinder (Airgas, concentration analyzed 4/17/2013) with a concentration of 514.5 (\pm 2%) ppm NO₂ in N₂. Approximately 300 ppb VOCs (typical VOCs used are Δ -carene, limonene, α -pinene or β -pinene) were generated by flowing zero air over a chilled liquid sample of VOC in a three-necked round bottom flask.

Ozone, zero air, and NO₂ flows were allowed to stabilize inside the chamber prior to introducing VOC flow to initiate the experiment. All flows were then continuous until the completion of the experiment. Particle number and size data was collected using a Scanning Electron Mobility Sizing (SEMS, Brechtel Manufacturing, Inc.), connected via conductive silicone tubing to

Deleted: obtained using

Formatted: Font: (Default) Times New Roman, 10 pt, Not Bold, Font color: Auto, English (US)

Deleted: i

Formatted: Font: (Default) Times New Roman, 10 pt, Not Bold, Font color: Auto, English (US), Subscript

Formatted: Font: (Default) Times New Roman, 10 pt, Not Bold, Font color: Auto, English (US)

Formatted: Font: (Default) Times New Roman, 10 pt, Not Bold, Font color: Auto, English (US), Subscript

Formatted: Font: (Default) Times New Roman, 10 pt, Not Bold, Font color: Auto, English (US)

Deleted: These

Formatted: Subscript

Formatted: Font: (Default) Times New Roman, 10 pt, Not Bold, Font color: Auto, English (US)

Deleted: t measurement

Deleted: as well as

Formatted: Font: (Default) Times New Roman, 10 pt, Not Bold, Font color: Auto, English (US)

Deleted: since this is an ambient measurement

225 minimize particle losses. Ozone concentration was measured using a Dasibi Model 1003-AH ozone monitor or Teledyne Model T400.

3.3 Determination of oven temperature setpoints

Temperature ramps were performed on different mixtures of known gases to determine the appropriate setpoint temperatures for each of the three ovens. Temperature ramp results were used to identify the correct setpoints for each oven to achieve 230 complete dissociation for each species. Both HNO_3 and AN measurements were performed by flowing zero air over a pure liquid analyte sample. The AN standard used was isobutyl nitrate (Aldrich 96% purity). A pure liquid sample of PN could not be obtained, so a $\text{NO}_3 + \Delta\text{-3-carene}$ mixture containing PNs was synthesized in the chamber as described above. Because concentrations were very stable, ramps were performed at 5 °C/min. Normalized measured NO_2 concentrations are plotted against temperature in Figure 4 because absolute concentrations were different for each class of nitrate.

235 Complete dissociation of PNs occurred at a thermocouple temperature reading of 130 °C, ANs at 385 °C, and HNO_3 at 600°C. The HNO_3 oven setpoint was chosen to be 700°C to allow the quantification of interference from NO_3 dissociated from N_2O_5 in that channel. At 600°C, HNO_3 is completely dissociated, but there is only partial conversion of NO_3 to NO_2 , creating an interference in the hot channel in the TD-CRDS. At 700°C, HNO_3 is completely dissociated and NO_3 is completely converted to NO_2 . Note that the dissociation plateaus do not overlap with the beginning of the adjacent curve, confirming the 240 ability to quantitatively separate nitrate species by temperature.

3.4 Quantification and treatment of N_2O_5 interference

High concentration $\Delta\text{-3-carene}$ nitrate oxidation experiments in the REC chamber typically had 650 ppb O_3 and 400 ppb NO_2 . When high concentrations of O_3 and NO_2 are present, they react in the chamber to form N_2O_5 . This was verified by performing a temperature ramp from a chamber at low and high oxidant concentrations (Figure 5). N_2O_5 dissociates to produce two NO_2 245 products (see R3 and R4 below) across a broad temperature range, in contrast to the sharp dissociation curves for peroxy- or alkyl- nitrates, such that the presence of N_2O_5 removes the clear plateau between PNs dissociation and ANs and give an interference in both PNs and ANs channels. A chamber with low NO_x conditions (335 ppb O_3 and ~ 3 ppb NO_2) that was left to equilibrate for 56 minutes after addition of $\Delta\text{-carene}$ gave a maximum N_2O_5 concentration of 1.6 ppb. The resulting temperature ramp gives the expected dissociation curve, showing both PNs and ANs plateaus (Figure 5). In this case, there is 250 good separation between PNs and ANs, because N_2O_5 is lower in concentration. This N_2O_5 interference has been previously observed by Womack et al. 2017. Note that given the gradual dissociation of N_2O_5 across this full temperature range, the extent of the interference depends on the exact temperature setpoints, so any similar TD-based organonitrate instrument that may be operated in high- N_2O_5 conditions should characterize its individual N_2O_5 interference.

To measure the N_2O_5 interference such that it can be corrected for, we ran an experiment with only oxidants in the chamber 255 (Figure 6). The TD-CRDS detects one NO_2 molecule from the first dissociation of NO_2 from N_2O_5 (Reaction 3) either in Oven 3 (the PNs channel) or in Oven 2 (the ANs channel), and another NO_2 is observed when the released NO_3 fragment further

Formatted: Subscript

Deleted: .2

Deleted: the first

260 dissociates in the HNO_3 channel (Reaction 4). We note that due to its high reactivity and wall losses (especially the NO_3 fragment), as well as the likelihood that some N_2O_5 remained incompletely dissociated even at the ANs oven temperature, the total N_2O_5 detection is substantially less than 100% of the N_2O_5 concentration present in the chamber. We also emphasize that these percentages are specific to the configuration used in this characterization experiment: from the chamber containing the modeled N_2O_5 concentration used to determine these interference percentages, a 2-m Teflon inlet line led to the TD-CRDS instrument. A kinetic model paired with measurements of NO_2 and O_3 in order to predict N_2O_5 can be used to quantify the interferences in each channel for a given setup.



265 The result of N_2O_5 is an elevated baseline in each of the PNs, ANs, and HNO_3 channels before the VOC is added. If an accurate N_2O_5 measurement is available, the interference from N_2O_5 (and NO_3) can be subtracted out of each channel, and these pre-
270 VOC injection signals can be used to assess the likely lower inlet transmission of N_2O_5 and NO_3 vs. the more stable PNs, ANs, and HNO_3 . In the absence of a separate N_2O_5 measurement, kinetic modeling can be used to predict how much N_2O_5 will be formed in each experiment, which can then be subtracted out. For example, in chamber experiments, comparing modeled N_2O_5 amounts to the amounts of signal in the ANs, PANs, and HNO_3 channels before VOC is added can quantify what fraction of N_2O_5 appears in each channel. If Reaction 3 happens across the PNs and ANs temperature range (130–385 °C), and Reaction
275 4 between the ANs and HNO_3 range (385–700 °C), the sum of the signals from the ANs and PANs channels before addition of VOC should be equivalent to the N_2O_5 signal from the HNO_3 channel (from the NO_3 fragment of the N_2O_5 dissociating to NO_2). For the instrument application shown here, operating at UC Irvine in September 2019, 7% of the modeled N_2O_5 produced based on a model constrained to measured NO_2 and O_3 is detected in the PNs channel at 150 °C, and 28% in the ANs channel at 385 °C.

280 3.5 Determination of denuder efficiency

The activated carbon denuder was tested for efficient removal of gas phase molecules by flowing gas mixtures of single molecules diluted in zero air through the denuder. Gas mixtures were tested at several concentrations to determine if efficiency was concentration-dependent. Transmission of the denuder is defined to be the percentage of gas-phase molecules that passed through the denuder and were detected downstream when all should have been removed.

285 NO_2 transmission was tested in 2016 at two relatively low concentrations, to mimic atmospheric conditions, and one higher concentration to mimic chamber conditions. In all cases at this time, greater than 96% of the NO_2 was absorbed (Table 1). NO_2 concentrations ranged from 26 to 271 ppb. In 2019, NO_2 transmission was again tested to assess changes in denuder performance over time, at 275 ppb. The larger observed NO_2 transmission in 2018 suggests a drift in the gas-phase breakthrough over time. Because transmission appears to change over time, we recommend making periodic measurements
290 and updating correction factors accordingly. Denuders can be cleaned by gentle heating and zero air flow.

Formatted: Subscript

Formatted: Subscript

Deleted: at the inlet

Formatted: Subscript

Formatted: Subscript

Table 1. Effect of inserting a single channel activated carbon denuder in between an NO₂ source and the TD-CRDS. [Errors were measured for the 2016 measurements and are reported as the standard deviation.](#)

Year	↓NO ₂] (ppb)	NO ₂ denuder transmission
2016	26	(3.3±0.3) %
2016	46	(3.1±0.2) %
2016	271	(1.96±0.08) %
2019	275	7.7 %

Deleted: are

Deleted: [NO₂] (ppb) 2016

Deleted:

Deleted: 2019

Formatted Table

Deleted: 26

Deleted: 46

Deleted: 271

Deleted: 2.0

295

The same process was used to determine the transmission of isobutyl nitrate (an alkyl nitrate) in 2016 (Table 2). The outlet of the denuder was connected to both Channel 1 (temporarily at 520°C) and Channel 2 (385°C). The transmission of the denuder was not dependent on the concentration of gas in the original gas mixture, or on which oven was used. This ANs transmission was also re-tested in 2019, and in this case, no significant change in breakthrough was observed. These measured fractions of 300 gas-phase breakthrough can be used to correct the aerosol measurements made in the denuded channels of the instrument cycle (see corrections discussion below).

Table 2. Transmission of denuder at three concentrations of isobutyl nitrate (IBN) and one concentration of chamber-generated AN. Transmission is defined as the percentage of gas-phase alkyl nitrate that was passed through the denuder. [Errors for the 2016 measurements are the standard deviation.](#)

Year	AN source	Concentration (ppb)	Transmission through
			Channel 2 (385°C)
2016	JBN	250	(13.2±0.3) %
2016	IBN	385	(11.0±0.4) %
2016	IBN	800	(12.8±0.2) %
2019	Δ-3-carene	35	11.0 %

Deleted: 1

Deleted: IBN

Deleted: 1

Deleted: Concentration IBN (ppb) 2016

Deleted: chamber ANs

Deleted: 2019

Deleted: 250

Deleted: 385

Deleted: 800

A chamber experiment with Δ-carene was performed to generate organic aerosol particles in order to test the aerosol throughput of the denuder. Low NO_x chamber conditions (450 ppb O₃, 3 ppb NO₂) were used to minimize potential N₂O₅ interferences. First, the chamber was hooked directly to the SEMS in order to get a background measure for the number of particles in the 310 bag. Then the chamber mixture was pulled through the TD-CRDS inlet tubing while bypassing the denuder in order to quantify particle losses to the tubing. Finally, the chamber mixture was sampled while flowing through the tubing and the denuder to get the total particle loss through the instrument. The time series of this experiment is shown in Figure 7. In order to quantify the efficiency of the denuder and tubing inlet of the TD-CRDS, the particle volume was averaged over the sampling time under each condition. This assumes particle concentration in the chamber was constant over the course of the entire experiment.

Since the chamber had been running for 24 hours prior to measurements, it is reasonable to assume that all concentrations had reached equilibrium.

A total of 28% of the aerosol particles (assessed by volume) that flow into the instrument were lost to the tubing and the denuder before detection. There does not appear to be any bias toward removing smaller or larger particles. The denuder is responsible for only 10% of total particle loss. This suggests that every deployment of this instrument should carefully consider and if possible quantify inlet line losses.

3.6 Determination of detection limits

The CRDS can be set to zero automatically at regular intervals, which is accomplished by diverting inlet air through an NO₂ scrubber. [The instrument is typically set to run its 3 minute zero every two hours](#). The re-zeroing procedure results in small changes to the baseline before and after zeroing events. On ambient measurements, these changes are typically less than 0.5 ppb (see Figure S3), and on zero air, typically less than 0.2 ppb, and are sometimes positive and sometimes negative. We determine the standard deviation of four hours of zero measurements (0.16 ppb) to estimate our blank error, σ_{zero} .

From this observed blank error, the detection limit of the instrument (LOD = 3 σ) can be calculated for each channel. The error for the NO₂ channel is based only on σ_{zero} alone, since no subtraction is required ($3\sigma_{\text{zero}} = 3 \times 0.16 \text{ ppb} = 0.48 \text{ ppb}$). For all other channels, the error in the subtracted value A - B is calculated as:

$$\sigma_{A-B} = \sqrt{(\sigma_A^2 + \sigma_B^2)} \quad (\text{Eq. 3})$$

where $\sigma_A = \sigma_B = 0.16 \text{ ppb}$ are the errors in the pre-subtraction NO₂ concentration measurements. Thus, the estimated detection limit for the subtracted channels (ANs, PNs, and HNO₃), $3\sigma_{A-B} = 3 \times 0.22 \text{ ppb} = 0.66 \text{ ppb}$.

355 3.7 Kinetic modelling of thermal dissociation ovens

Modelling of the ovens can be employed to simulate the dissociation and recombination of the detected species in any oven design. Pressure- and temperature-dependent rate constants for dissociation ([Day et al. 2002](#)) and recombination ([JPL Data Evaluation 2015](#)) reactions of PNs, ANs, and HNO₃ were used (see Table S1), alongside an assumed (a) step function or (b) linear rate of cooling from the heated to the unheated portions of the oven (see Figure S4). We also included the IUPAC rate constant for a representative RO + O₂ ($7.2 \times 10^{-14} e^{1080/T}$, [IUPAC](#)), and OH wall loss rate ([calculated to be 46 s⁻¹ for these conditions](#)) from Knopf, Pöschl, and Shiraiwa 2015. Based on these rate constants and the assumption that recombination or wall losses are the only fates for dissociated radicals, we found that the PNs measurement would be the most affected by recombination. We found an expected 10% difference in the amount of PNs recombined by the end of the PNs oven between assuming linear cooling and step function, so the more conservative step function assumption can be used to provide a lower limit concentration.

All ovens were modelled at their setpoint temperature, which is maintained by the thermocouple relay. However, each oven surely has gradients in temperature along its length, resulting in this average oven temperature measured at its midpoint (see

Formatted: Font: (Default) Times New Roman, 10 pt, Not Bold, Font color: Auto, English (US)

Formatted: Font: (Default) Times New Roman, 10 pt, Not Bold, Font color: Auto, English (US)

Deleted: 46 s⁻¹

Deleted: (

Deleted:)

Deleted: Knopf, Pöschl, and Shiraiwa 2015

Figure 1b). As an example, for HNO_3 there was very little difference in dissociation based on small changes in oven temperature. HNO_3 is 100% dissociated at the end of the oven, so modelling at 30°C hotter than the setpoint temperature just 375 extends the cooling region slightly. This leads to approximately 0.3% less recombination than the setpoint temperature model.

The same concept applies to the PNs oven, but the recombination difference is larger (1-2% depending on model molecule) due to a 30°C increase in temperature being a larger percentage of the total temperature.

The PN dissociation and recombination oven model results in Figure S5 show a predicted 55.9% dissociation in the step function model, and 65.4% dissociation in the linear function model with no background NO_2 and 10 ppb initial PNs 380 concentration.

In the PNs oven, the only important reactions modelled were the dissociation and recombination of PNs. The background concentration of NO_2 was considered and was found to have a significant impact on the recombination rate, especially at high concentrations. Figure S6 shows the percent PNs that remain dissociated at the detector as a function of initial concentrations 385 of PNs and NO_2 . Two separate types of PN were considered in the modelling, due to their slightly different rates of recombination. Methyl PN gave 58.1% detection at 10 ppb initial concentration and no background NO_2 , while ethyl PN gave 55.9% detection under the same conditions. Given the relatively small difference in recombination percentages, no effort was made to incorporate both species into the model. Ethyl PN was chosen as the representative species because it was assumed that most PNs being encountered would be two carbons or larger. Including reasonable atmospheric concentrations of OH (4x10⁶ molecules /cm³) in the model made no difference to the percent recombination of ethyl PNs, and was therefore left out.

390 We note that the PNs measurement will be most affected by recombination, but that this recombination can in principle be corrected for.

In addition to the potential reduction in PNs signal due to recombination reactions, there is the potential for a spurious overestimation of PNs signal due to reactions of thermally dissociated peroxy or peroxy acetyl radicals with ambient NO in the presence of O_2 , producing additional NO_2 (Thieser et al. 2016). This effect will be minimal in chamber simulations of nighttime chemistry, where the mixing ratio of NO is zero, but should be considered in any daytime field deployments.

In the ANs oven, in addition to the major reactions of ANs dissociation and recombination, the reaction $\text{RO} + \text{O}_2$ is also 400 important. The $\text{RO} + \text{O}_2$ reaction is extremely fast at high temperatures (see Table S1) like those found in the heated portion of the AN oven, and we assume the reaction to be irreversible. Because O_2 is abundant, the reaction negligibly affects O_2 concentration. As a result, these assumptions give a model prediction of 100% detection of alkyl nitrates at all initial AN and NO_2 concentrations.

In the HNO_3 oven, in addition to the dissociation and recombination of HNO_3 , the loss of OH radical to the walls is significant, competing with recombination. The model assumes that any OH that hits the walls after the heating part of the oven is lost due to reactions with the walls; as a result, recombination is generally less of an effect on the HNO_3 measurement. Figure S7 shows example model outputs for the HNO_3 oven, predicting the percent dissociation of HNO_3 at the point of detection over 405 a large range of initial concentrations for both HNO_3 and NO_2 . As expected, recombination is most important at larger NO_2 and HNO_3 concentrations; below 50 ppb of each, for this instrument configuration the detection efficiency is above 80%.

Deleted: 5 show

Formatted: Subscript

Formatted: Subscript

Formatted: Not Superscript/ Subscript

Formatted: Not Superscript/ Subscript

Deleted: 

Formatted: Font: Bold

3.8 Ozone pyrolysis at high temperatures interferes with HNO₃ measurement

410 One additional reaction that can affect the HNO₃ measurement is the pyrolysis of O₃. At high temperatures, some fraction of O₃ dissociates, releasing atomic O which reacts with NO₂ to form NO + O₂, which results in NO₂ being removed from the final measurement. Therefore, in background conditions of high O₃ concentration, the NO₂ concentrations measured after the HNO₃ oven are biased low and can even cause the [HNO₃] to appear negative upon subtraction. [Day et al. 2002](#) noted that at or above 530 °C, all O₃ will separate into O₂ and O molecules, which will then react with NO₂. This suggests that for 415 this instrument, the pyrolysis of O₃ will result in a lower signal only in Oven 1 (700 °C) due to the high temperatures.

420 In some experiments from the 2018 SAPHIR NO₃ISOP campaign, HNO₃ measurements appeared negative due to lower signals from the hottest channel. Using other available instruments' measurements of O₃ and HNO₃, we determined that approximately 4% of the O₃ signal was converted to this apparent negative HNO₃ signal during one experiment (on 8-Aug-2018). However, this fraction did not appear consistent across experiments, perhaps due to substantial HNO₃ inlet losses, and 420 we did not determine a robust and consistent correction factor for this effect. Given that this does not affect alkyl nitrate measurements, and that there were other measurements of HNO₃ available, we did not pursue this further. But in principle, this is a relatively modest effect that can be corrected for after experimentally determining the efficiency of ozone pyrolysis for a particular inlet oven build.

3.9 Data corrections

425 The above modeled 100% efficiency in detecting ANs is fortunate, since the ANs measurement has thus far been the output of greatest interest from this instrument. Should one wish to use such an instrument for accurate measurements of PNs and HNO₃, this too is possible, but requires the determination of correction factors to account for the recombination in those ovens. Beyond the correction factors for radical recombination in the cooling region after each oven (1), additional corrections that 430 can be applied are: (2) oven-specific denuder breakthrough, based on data such as that shown in Tables 1 and 2, (3) background corrections, to account for any background signal detected in each channel while sampling zero air (this could account for inlet and/or denuder offgassing), (4) subtraction of N₂O₅ interference, as described in section 3.4 above, and (5) correction of the HNO₃ channel for O₃ pyrolysis loss of NO₂, as described in section 3.8 above. The importance of each of these corrections will depend on the nature of the experiments conducted; some example applications are shown below to illustrate this.

435 We have implemented each of these corrections as optional to apply to any raw data collected in our Igor-based data workup routine, which also sorts the data from the various ovens, averages, and subtracts the relevant signals.

4 Representative uses of the TD-CRDS

4.1 AMS / TD-CRDS aerosol terpene nitrate comparison at CU Boulder chamber

The TD-CRDS was compared to the CU Boulder Jimenez group aerosol mass spectrometer (AMS) during collaborative chamber experiments in Summer 2015, using the data from the denuded ANs channel of the TD-CRDS and the high-resolution AMS organic nitrate (pRONO₂) measurement to assess the correlation of these two aerosol-phase organic nitrate measurements. The experiments plotted here are those which showed substantial aerosol nitrate formation using Δ-carene or α-pinene as a VOC precursor and NO₃ from an N₂O₅ trap, both spanning the nominal range of 10-100 ppb, at varying relative humidity. The comparison of individual measurements across two weeks of experiments show significant scatter, but an orthogonal distance regression (ODR) fit to the scatterplot of TD-CRDS data vs. AMS data shows a slope of about 0.88-0.94 (depending on intercept treatment), and R²=0.73 (Figure 8).

The AMS organic nitrate concentrations in Figure 9 were calculated by apportioning the total nitrate concentration using the NO_x⁺ ion ratio (NO₂⁺/NO⁺) method ([Farmer et al. 2010](#)), where the relative ratios of organic to inorganic NO_x⁺ ratios (“ratio-of-ratios”; [Fry et al. 2013](#)) were determined by the average of several dry, unseeded experiments and ammonium nitrate ratios from offline calibrations (3.12 for Δ-carene, 3.78 for α-pinene). The organic-inorganic separation was conducted in order to account for possible NH₄NO₃ or particle HNO₃ formation as was suggested by substantial shifts in NO_x⁺ ratios observed during wet, seeded experiments, as has been reported previously ([Takeuchi and Ng 2019](#)). Figure S8 shows a comparison of the Figure 8 results to a plot of the TD-CRDS measurements against the AMS total nitrate (unapportioned), the latter resulting in slightly lower slopes and correlation coefficients.

Previous comparisons between AMS and thermal dissociation-based aerosol organic nitrate instruments have found varying agreement for ambient measurements ([Ng et al. 2017](#)). Some of these differences could be due to the fact that the ambient atmosphere contains a mix of diverse products from the oxidation of monoterpenes and isoprene in the presence of other gases; the resulting differing mixes of alkyl nitrate structures could alter the sensitivity of one or both instruments.

Deleted: 1

4.2 Ambient measurements of organonitrates in Portland, OR

During one week in November 2014, the TD-CRDS inlet was situated outside the south end of the Reed College Chemistry building. Simultaneous measurements of NO₂, PNs, ANs, and HNO₃ were made and one representative day is shown in Figure 9, illustrating typical measurable ambient variability and diurnal cycle.

4.3 Chamber measurements of isoprene nitrates at SAPHIR chamber (Jülich, Germany)

The TD-CRDS was also used in the month-long SAPHIR NO₃ + isoprene campaign in the summer of 2018. The Simulation of Atmospheric Photochemistry in a Large Reaction Chamber (SAPHIR) is a 270 m³ double-walled Teflon chamber with movable shutters allowing for simulation of both daytime and nighttime chemistry. The experiments were run in batch mode with periodic injections of oxidants and reactants. The reactant concentrations were comparable to real atmospheric

concentrations of NO_2 , O_3 , and isoprene. Some experiments were run under humid conditions and some had seed aerosol added
470 to facilitate condensations of gas products into the particle phase.

The low, near-ambient concentrations of reactants used, the small degree of partitioning of isoprene nitrates to the aerosol
phase, and the relatively long inlet line required resulted in the aerosol organonitrate products being lower than the limit of
detection of the TD-CRDS for the particle-phase ANs monitoring. The gas-phase ANs measurements from the TD-CRDS
475 ranged from sub-ppb up to 16 ppb of organic nitrates, with an observed alkyl nitrate molar yield for $\text{NO}_3 +$ isoprene of ~ 100%
under all explored reaction conditions. In order to determine gas/aerosol partitioning of nitrates, the gas-phase ANs measured
by TD-CRDS were compared to AMS organic nitrate aerosol measurement. These results are the subject of a forthcoming
paper (Brownwood et al., in preparation, 2020).

4.4 Chamber measurements of isoprene nitrates at REC (Portland, OR)

The TD-CRDS was also used for chamber experiments throughout the 2018-2019 academic year at the Reed Environmental
480 Chamber (REC), running experiments similar to those from SAPHIR, but at substantially higher concentrations. These
experiments aimed to determine whether gas-particle partitioning coefficients (K_p) for the NO_3 -initiated oxidation of isoprene
would be similar in a 0.4 m^3 chamber at much higher concentrations to those measured in the 270 m^3 SAPHIR chamber at
much lower, near-ambient concentrations.

The gas-particle partitioning coefficients calculated in these experiments used the aerosol and total gas + aerosol measurements
485 from the TD-CRDS and a total mass measurement from a Brechtel SEMS (BMIT Model 2002). The partitioning coefficients
derived from these experiments were 5×10^{-4} and $4.4 \times 10^{-3} \text{ m}^3 \mu\text{g}^{-1}$, for background aerosol loadings of 230 and 20 $\mu\text{g m}^{-3}$,
respectively. One of these experiments is shown in Figure 10. The aerosol (c_{aer}) and total ANs concentrations, and background
aerosol loading (M_{tot}) were averaged over the shaded period, aerosol-phase was subtracted from total to obtain c_{gas} , from which
490 K_p was determined via Equation 4:

$$490 \quad K_p = \frac{c_{aero}}{c_{gas} M_{tot}} \quad (\text{Eq. 4})$$

The fact that the two experiments at different background aerosol mass loadings (M) did not give exactly the same K_p value
495 could reflect the uncertainty of these measurements, or that the aerosol partitioning is not perfectly described as absorptive
partitioning, or that wall losses change as aerosol loadings change. Most important, the range of K_p measured here fall exactly
within the range of values observed over a month of $\text{NO}_3 +$ isoprene experiments conducted under much lower concentration
conditions at the SAPHIR chamber ($5 \times 10^{-4} - 6 \times 10^{-3} \text{ m}^3 \mu\text{g}^{-1}$, Brownwood et al., in preparation, 2020)

These K_p values were compared to theoretical calculations of K_p predicted by the simplified p^o_L prediction (SIMPOL.1) group
500 contribution method (Pankow and Asher 2008), and we find this average volatility consistent with a tri-functional isoprene
nitrates, such as isoprene hydroperoxy nitrate, which has a SIMPOL.1 predicted K_p value of $2.38 \times 10^{-3} \text{ m}^3 \mu\text{g}^{-1}$. This shows a
promising consistency of equilibrium gas-aerosol partitioning of isoprene nitrate products measured in two dramatically
different chambers, and suggests the robustness of the TD-CRDS over a wide range of concentrations.

5 Conclusions

Using three custom home-built oven channels, a charcoal denuder, and an automated valve control system, a thermal dissociation cavity ringdown spectrometer (TD-CRDS) was constructed for the speciated measurement of gas- and aerosol-phase organic nitrates, split into the classes NO₂, PN_s, AN_s, and HNO₃. This instrument has been successfully demonstrated

505 for measurements on atmospheric simulation chambers operating at a wide range of concentrations and ambient measurements; because of the increased uncertainty in the presence of rapid background changes in NO₂ mixing ratio, the TD-CRDS is best suited to chamber studies. Users or developers of similar such instruments are encouraged to consider the several data corrections described herein, which will be more or less important depending on the details of the instrument deployment.

Formatted: Subscript

Acknowledgements

510 The authors acknowledge many fruitful conversations with a large number of collaborators, with whom we have enjoyed working as we built and refined this instrument. We thank colleagues at University of Colorado at Boulder: Jose Jimenez, Hyungu Kang, Jason Schroder and Pedro Campuzano-Jost, for sharing AMS data and stimulating discussions during our work together in 2014-2015. Keehan, Day and Fry acknowledge support for this collaboration from NOAA's Climate Program Office's Atmospheric Chemistry, Carbon Cycle, and Climate program Grant # NA13OAR4310070. We also thank colleagues
515 at UC Irvine: Jim Smith, Danielle Draper, and Lia Damm, for stimulating discussions during our work together in 2019-2020. Marsavin, Brownwood, and Fry acknowledge support from the U.S. National Science Foundation (NSF) under Grant # AGS-1762106. We thank Reed College colleagues Ben Ayres and Jay Ewing, and Paul Wooldridge and Ron Cohen (UC Berkeley) for valuable discussions and help with instrument construction, and John Crowley and his students (Max Planck Institute for Chemistry, Mainz, Germany) for many valuable discussions around our work together at Forschungszentrum Jülich in 2018.

520 References

Atkinson, R., D. L. Baulch, R. A. Cox, J. N. Crowley, R. F. Hampson, R. G. Hynes, M. E. Jenkin, M. J. Rossi, J. Troe, and IUPAC Subcommittee. 2006. "Evaluated Kinetic and Photochemical Data for Atmospheric Chemistry: Volume II -- Gas Phase Reactions of Organic Species." *Atmospheric Chemistry and Physics* 6 (11): 3625–4055. <https://doi.org/10.5194/acp-6-3625-2006>.

525 Browne, E. C., K.-E. Min, P. J. Wooldridge, E. Apel, D. R. Blake, W. H. Brune, C. A. Cantrell, et al. 2013. "Observations of Total RONO₂ over the Boreal Forest: NO_x Sinks and HNO₃ Sources." *Atmospheric Chemistry and Physics* 13 (9): 4543–62. <https://doi.org/10.5194/acp-13-4543-2013>.

Buhr, Martin P., David D. Parrish, Richard B. Norton, Frederick C. Fehsenfeld, Robert E. Sievers, and James M. Roberts. 1990. "Contribution of Organic Nitrates to the Total Reactive Nitrogen Budget at a Rural Eastern U.S. Site." *Journal of*
530 *Geophysical Research: Atmospheres* 95 (D7): 9809–16. <https://doi.org/10.1029/JD095iD07p09809>.

Deleted: {Citation}

Deleted: –

Deleted: ;

Day, D. A., P. J. Wooldridge, M. B. Dillon, J. A. Thornton, and R. C. Cohen. 2002. "A Thermal Dissociation Laser-Induced 535 Fluorescence Instrument for in Situ Detection of NO₂, Peroxy Nitrates, Alkyl Nitrates, and HNO₃." *Journal of Geophysical Research-Atmospheres* 107 (D5-6): 4046, doi:10.1029/2001JD000779. <https://doi.org/doi:10.1029/2001JD000779>.

Draper, D. C., D. K. Farmer, Y. Desyaterik, and J. L. Fry. 2015. "A Qualitative Comparison of Secondary Organic Aerosol 540 Yields and Composition from Ozonolysis of Monoterpenes at Varying Concentrations of NO₂." *Atmospheric Chemistry and Physics* 15 (21): 12267–81. <https://doi.org/10.5194/acp-15-12267-2015>.

545 Farmer, D. K., A. Matsunaga, K. S. Docherty, J. D. Surratt, J. H. Seinfeld, P. J. Ziemann, and J. L. Jimenez. 2010. "Response of an Aerosol Mass Spectrometer to Organonitrates and Organosulfates and Implications for Atmospheric Chemistry." *Proceedings of the National Academy of Sciences* 107 (15): 6670–75. <https://doi.org/10.1073/pnas.0912340107>.

Fry, J. L., D. C. Draper, K. J. Zarzana, P. Campuzano-Jost, D. A. Day, J. L. Jimenez, S. S. Brown, et al. 2013. "Observations 550 of Gas- and Aerosol-Phase Organic Nitrates at BEACHON-RoMBAS 2011." *Atmospheric Chemistry and Physics* 13 (17): 8585–8605. <https://doi.org/10.5194/acp-13-8585-2013>.

Glasius, Marianne, Morten Funch Carlsen, Torben Stroyer Hansen, and Christian Lohse. 1999. "Measurements of Nitrogen 555 Dioxide on Funen Using Diffusion Tubes." *Atmospheric Environment* 33 (8): 1177–85. [https://doi.org/10.1016/S1352-2310\(98\)00285-4](https://doi.org/10.1016/S1352-2310(98)00285-4).

Hao, Cunsheng., Paul B. Shepson, John W. Drummond, and Kayambu. Muthuramu. 1994. "Gas Chromatographic Detector 560 for Selective and Sensitive Detection of Atmospheric Organic Nitrates." *Analytical Chemistry* 66 (21): 3737–43. <https://doi.org/10.1021/ac00093a032>.

Hargrove, James, and Jingsong Zhang. 2008. "Measurements of NO_x, Acyl Peroxynitrates, and NO_y with Automatic 565 Interference Corrections Using a NO₂ Analyzer and Gas Phase Titration." *The Review of Scientific Instruments* 79 (4): 046109. <https://doi.org/10.1063/1.2908432>.

570 Horowitz, Larry W., Arlene M. Fiore, George P. Milly, Ronald C. Cohen, Anne Perring, Paul J. Wooldridge, Peter G. Hess, Louisa K. Emmons, and Jean-François Lamarque. 2007. "Observational Constraints on the Chemistry of Isoprene Nitrates over the Eastern United States." *Journal of Geophysical Research: Atmospheres* 112 (D12). <https://doi.org/10.1029/2006JD007747>.

IUPAC. n.d. "Task Group on Atmospheric Chemical Kinetic Data Evaluation." Accessed April 22, 2020. <http://iupac.pole-ether.fr/>.

575 Jimenez, J. L., M. R. Canagaratna, N. M. Donahue, A. S. H. Prevot, Q. Zhang, J. H. Kroll, P. F. DeCarlo, et al. 2009. "Evolution of Organic Aerosols in the Atmosphere." *Science* 326 (5959): 1525–29. <https://doi.org/10.1126/science.1180353>.

JPL Data Evaluation. 2015. JPL Data Evaluation, Number 18. October 2015. <https://jpldataeval.jpl.nasa.gov/>.

580 Kim, Yoo Jung, Scott N. Spak, Gregory R. Carmichael, Nicole Riemer, and Charles O. Stanier. 2014. "Modeled Aerosol Research: Atmospheres 119 (21): 12,420-12,445. <https://doi.org/10.1002/2014JD022320>.

Kirchner, F., A. Mayer-Figge, F. Zabel, and K. H. Becker. 1999. "Thermal Stability of Peroxynitrates." *International Journal of Chemical Kinetics* 31 (2): 127–44. [https://doi.org/10.1002/\(SICI\)1097-4601\(1999\)31:2<127::AID-KIN>3.0.CO;2-L](https://doi.org/10.1002/(SICI)1097-4601(1999)31:2<127::AID-KIN>3.0.CO;2-L).

Knopf, Daniel A., Ulrich Pöschl, and Manabu Shiraiwa. 2015. "Radial Diffusion and Penetration of Gas Molecules and 570 Aerosol Particles through Laminar Flow Reactors, Denuders, and Sampling Tubes." *Analytical Chemistry* 87 (7): 3746–54. <https://doi.org/10.1021/ac504239s>.

Lee, Ben H., Claudia Mohr, Felipe D. Lopez-Hilfiker, Anna Lutz, Mattias Hallquist, Lance Lee, Paul Romer, et al. 2016. "Highly Functionalized Organic Nitrates in the Southeast United States: Contribution to Secondary Organic Aerosol and Reactive Nitrogen Budgets." *Proceedings of the National Academy of Sciences* 113 (6): 1516–21. 575 <https://doi.org/10.1073/pnas.1508108113>.

Ng, Nga Lee, Steven S. Brown, Alexander T. Archibald, Elliot Atlas, Ronald C. Cohen, John N. Crowley, Douglas A. Day, et al. 2017. "Nitrate Radicals and Biogenic Volatile Organic Compounds: Oxidation, Mechanisms, and Organic Aerosol." *Atmospheric Chemistry and Physics* 17 (3): 2103–62. <https://doi.org/10.5194/acp-17-2103-2017>.

Pankow, J F, and W E Asher. 2008. "SIMPOL.1: A Simple Group Contribution Method for Predicting Vapor Pressures and 580 Enthalpies of Vaporization of Multifunctional Organic Compounds." *Atmos. Chem. Phys.*, 24.

Parrish, David D, and Fred C Fehsenfeld. 2000. "Methods for Gas-Phase Measurements of Ozone, Ozone Precursors and Aerosol Precursors." *Atmospheric Environment* 34 (12): 1921–57. [https://doi.org/10.1016/S1352-2310\(99\)00454-9](https://doi.org/10.1016/S1352-2310(99)00454-9).

Paul, D., A. Furgeson, and H. D. Osthoff. 2009. "Measurements of Total Peroxy and Alkyl Nitrate Abundances in Laboratory-Generated Gas Samples by Thermal Dissociation Cavity Ring-down Spectroscopy." *Review of Scientific Instruments* 80 (11). 585 <https://doi.org/10.1063/1.3258204>.

Peng, Zhe, and Jose L. Jimenez. 2019. "KinSim: A Research-Grade, User-Friendly, Visual Kinetics Simulator for Chemical-Kinetics and Environmental-Chemistry Teaching." *Journal of Chemical Education* 96 (4): 806–11. <https://doi.org/10.1021/acs.jchemed.9b00033>.

Perring, A. E., S. E. Pusede, and R. C. Cohen. 2013. "An Observational Perspective on the Atmospheric Impacts of Alkyl and 590 Multifunctional Nitrates on Ozone and Secondary Organic Aerosol." *Chemical Reviews*. <https://doi.org/10.1021/cr300520x>.

Rollins, A. W., J. D. Smith, K. R. Wilson, and R. C. Cohen. 2010. "Real Time In Situ Detection of Organic Nitrates in Atmospheric Aerosols." *Environmental Science & Technology* 44 (14): 5540–45. <https://doi.org/10.1021/Es100926x>.

Seinfeld, John H., and Spyros N. Pandis. 2006. *Atmospheric Chemistry and Physics: From Air Pollution to Climate Change*. 2nd ed. Hoboken, N.J: J. Wiley.

595 Seinfeld, John H., and James F. Pankow. 2003. "Organic Atmospheric Particulate Material." *Annual Review of Physical Chemistry* 54 (1): 121–40. <https://doi.org/10.1146/annurev.physchem.54.011002.103756>.

Sobanski, Nicolas, Jan Schuladen, Gerhard Schuster, Jos Lelieveld, and John N. Crowley. 2016. "A Five-Channel Cavity Ring-down Spectrometer for the Detection of NO₂, NO₃, N₂O₅, Total Peroxy Nitrates and Total Alkyl Nitrates." *Atmospheric Measurement Techniques* 9 (10): 5103–18. <https://doi.org/10.5194/amt-9-5103-2016>.

Field Code Changed

Formatted: Font: (Default) Times New Roman, 10 pt

Formatted: Font: (Default) Times New Roman, 10 pt

600 Surratt, Jason D., Shane M. Murphy, Jesse H. Kroll, Nga L. Ng, Lea Hildebrandt, Armin Sorooshian, Rafal Szmigielski, et al. 2006. "Chemical Composition of Secondary Organic Aerosol Formed from the Photooxidation of Isoprene." *The Journal of Physical Chemistry. A* 110 (31): 9665–90. <https://doi.org/10.1021/jp061734m>.

Takeuchi, Masayuki, and Nga L. Ng. 2019. "Chemical Composition and Hydrolysis of Organic Nitrate Aerosol Formed from Hydroxyl and Nitrate Radical Oxidation of α -Pinene and β -Pinene." *Atmospheric Chemistry and Physics* 19 (19): 12749–66. <https://doi.org/10.5194/acp-19-12749-2019>.

605 Thornton, J. A., P. J. Wooldridge, R. C. Cohen, M. Martinez, H. Harder, W. H. Brune, E. J. Williams, et al. 2002. "Ozone Production Rates as a Function of NO_x Abundances and HO_x Production Rates in the Nashville Urban Plume." *Journal of Geophysical Research: Atmospheres* 107 (D12): ACH 7-1-ACH 7-17. <https://doi.org/10.1029/2001JD000932>.

Williams, E. J., K. Baumann, J. M. Roberts, S. B. Bertman, R. B. Norton, F. C. Fehsenfeld, S. R. Springston, et al. 2012. 610 "Intercomparison of Ground-Based NO_y Measurement Techniques." *Journal of Geophysical Research: Atmospheres*, September, 22261–80. [https://doi.org/10.1029/98JD00074@10.1002/\(ISSN\)2169-8996.S0S1](https://doi.org/10.1029/98JD00074@10.1002/(ISSN)2169-8996.S0S1).

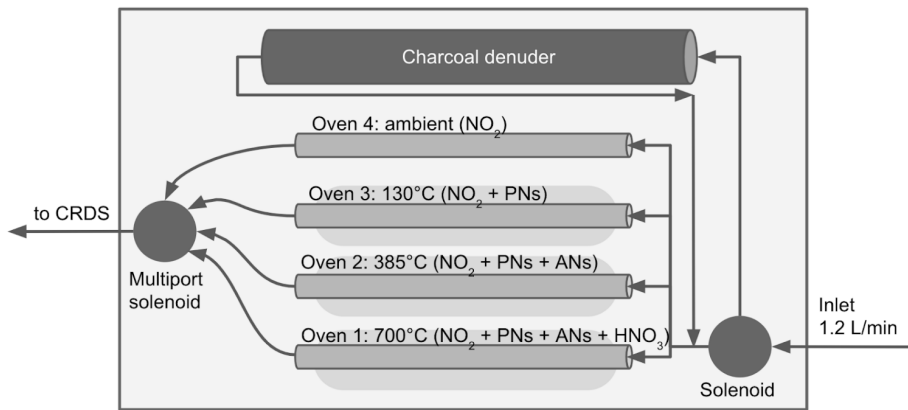
Wolfe, G. M., J. A. Thornton, V. F. McNeill, D. A. Jaffe, D. Reidmiller, D. Chand, J. Smith, P. Swartzendruber, F. Flocke, and W. Zheng. 2007. "Influence of Trans-Pacific Pollution Transport on Acyl Peroxy Nitrate Abundances and Speciation at Mount Bachelor Observatory during INTEX-B." *Atmospheric Chemistry and Physics* 7 (20): 5309–25. 615 <https://doi.org/10.5194/acp-7-5309-2007>.

Womack, Caroline C., J. Andrew Neuman, Patrick R. Veres, Scott J. Eilerman, Charles A. Brock, Zachary C. J. Decker, Kyle J. Zarzana, et al. 2017. "Evaluation of the Accuracy of Thermal Dissociation CRDS and LIF Techniques for Atmospheric Measurement of Reactive Nitrogen Species." *Atmospheric Measurement Techniques* 10 (5): 1911–26. <https://doi.org/10.5194/amt-10-1911-2017>.

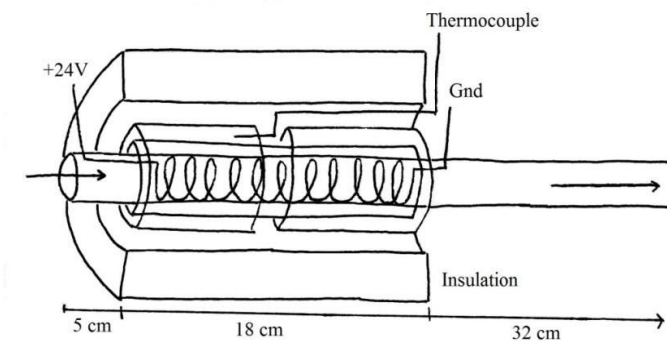
620 Wooldridge, P. J., A. E. Perring, T. H. Bertram, F. M. Flocke, J. M. Roberts, H. B. Singh, L. G. Huey, et al. 2010. "Total Peroxy Nitrates (Sigma PN)s in the Atmosphere: The Thermal Dissociation-Laser Induced Fluorescence (TD-LIF) Technique and Comparisons to Speciated PAN Measurements." *Atmospheric Measurement Techniques* 3 (3): 593–607. <https://doi.org/DOI 10.5194/amt-3-593-2010>.

Zare, Azimeh, Paul S. Romer, Tran Nguyen, Frank N. Keutsch, Kate Skog, and Ronald C. Cohen. 2018. "A Comprehensive 625 Organic Nitrate Chemistry: Insights into the Lifetime of Atmospheric Organic Nitrates." *Atmospheric Chemistry and Physics* 18 (20): 15419–36. <https://doi.org/10.5194/acp-18-15419-2018>.

Zellweger, C., M. Ammann, P. Hofer, and U. Baltensperger. 1999. "NO_y Speciation with a Combined Wet Effluent Diffusion Denuder – Aerosol Collector Coupled to Ion Chromatography." *Atmospheric Environment* 33 (7): 1131–40. [https://doi.org/10.1016/S1352-2310\(98\)00295-7](https://doi.org/10.1016/S1352-2310(98)00295-7).



a



b

Figure 1. (a) Diagram of thermal dissociation inlet flow path. The downstream valve is a Teflon-wetted six-solenoid multiport valve.
 635 (b) Oven design. Arrows indicate direction of airflow. A photograph of the inlet box is shown in the Supplemental Information, Figure S1.

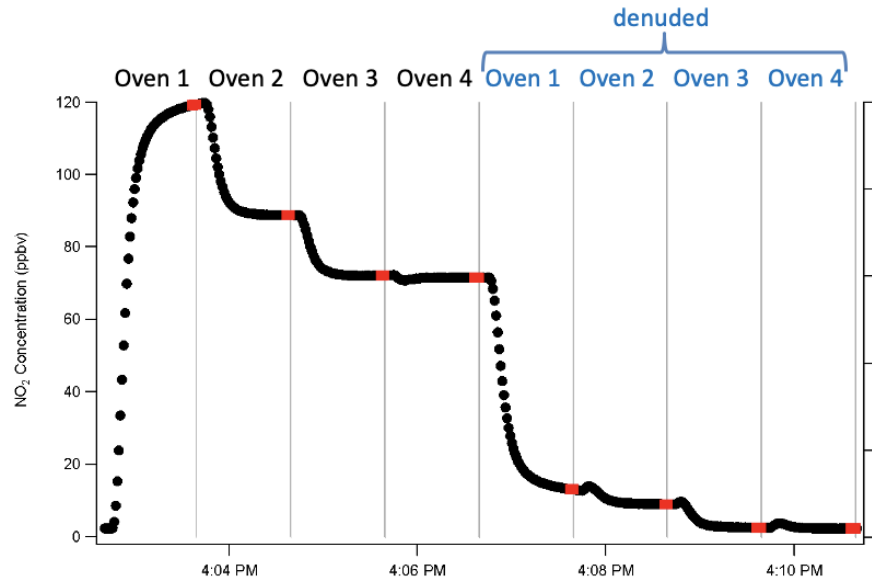


Figure 2. One full cycle through total and then denuded channels. Points indicated in red are those averaged to obtain the concentrations that are subsequently subtracted. Vertical lines indicate times when the valve switched between channels.

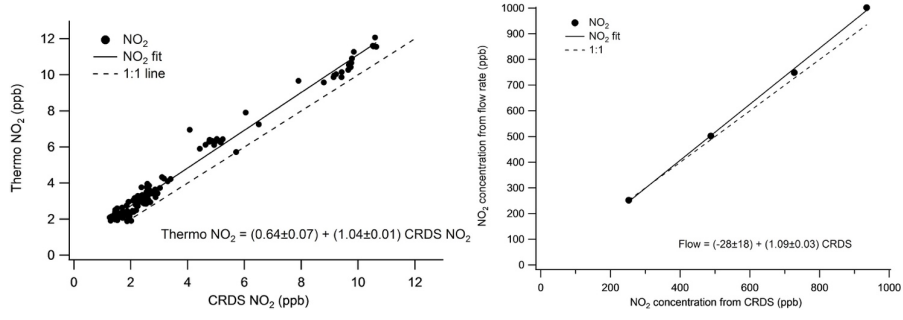
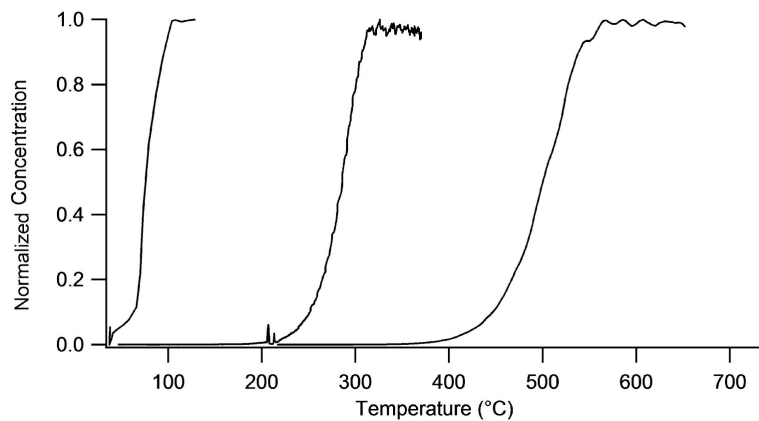
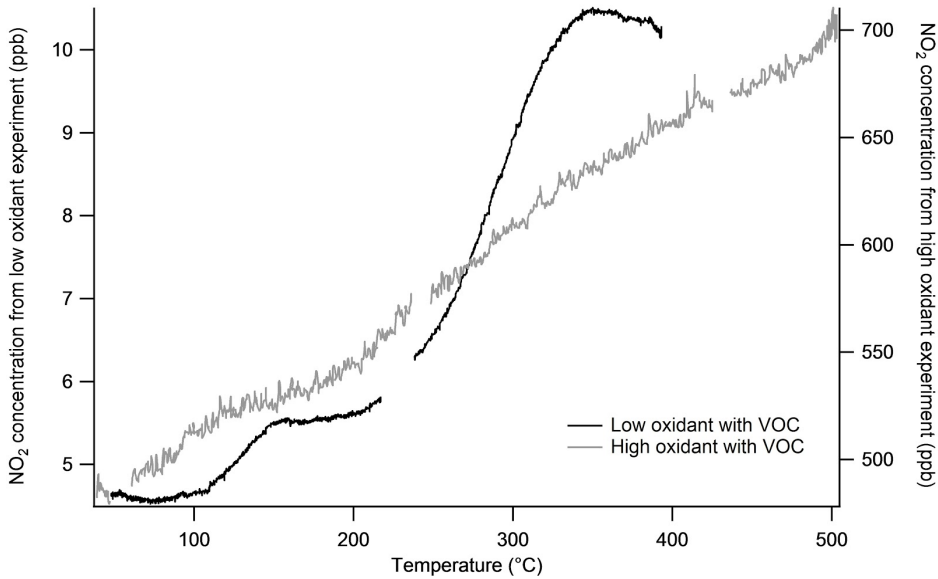


Figure 3. (left) Low concentration NO₂ comparison of Los Gatos Research NO₂ cavity ring-down spectrometer to a Thermo chemiluminescent NO_x box. The dashed line represents a 1:1 relationship. The slope of the fitted line is 1.04 ± 0.01 . (right) High concentration NO₂ comparison of LGR cavity ring-down spectrometer to concentrations calculated using flow rates. The dashed line is a 1:1 relationship. The slope of the fitted line is 1.09 ± 0.03 .



645

Figure 4. Temperature ramps on all thermally dissociated species, in order from left to right: chamber-generated PN, isobutyl nitrate and HNO₃ from pure samples diluted in zero air. The absolute concentrations of PN, AN, and HNO₃ were 230, 200, and 3000 ppb, respectively.



650 Figure 5. Comparison of two experiments under different initial NO_2 conditions to change the total N_2O_5 concentration. Both experiments contain 300 ppb Δ -carene. The ‘high oxidant’ experiment was performed with 650 ppb O_3 and 400 ppb NO_2 , which yields substantial N_2O_5 formation. The ‘low oxidant’ experiment was performed with 335 ppb O_3 and 3 ppb NO_2 , and reveals the clean separation of PN and ANs by plateaus. There are no distinct plateaus for PN and ANs in the high oxidant experiment, because they are washed out by the more gradually temperature-dependent dissociation of N_2O_5 .

Deleted: .2

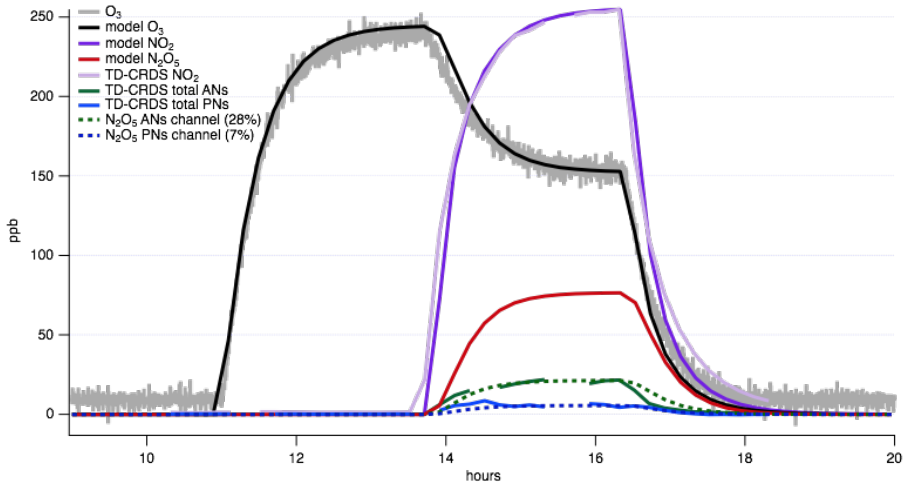


Figure 6: N_2O_5 contribution to TD-CRDS channels assessed by an oxidant-only chamber experiment. Allowing (measured) NO_2 and O_3 to stabilize sequentially enables prediction of N_2O_5 concentration (red trace) using a kinetics box model, such as KinSim (Peng and Jimenez 2019). Then, the signal in the PN and ANs channel of the TD-CRDS can be examined during the N_2O_5 rise time, and percentages can be applied to assess the fraction of N_2O_5 that is detected in each channel. For our TD-CRDS, this analysis reveals these percentages are 7% in the PN channel and 28% in the ANs channel.

660

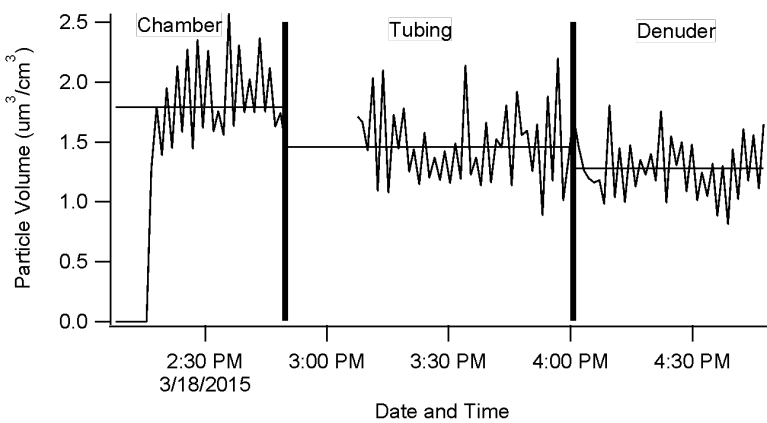


Figure 7. SEMS-measured particle volume versus time to test denuder efficiency. From 2:15 to 3:00 the SEMS was measuring directly from the chamber. From 3:00 to 4:00 the SEMS was measuring particles from the TD-CRDS tubing (only internal tubing to the inlet system) without the denuder. From 4:00 to 5:00 the SEMS measured through the TD-CRDS tubing and the denuder. The horizontal lines represent the average particle volume over the sampling period. The missing data was due to room air entering the lines while the SEMS was detached from the chamber and reattached to the TD-CRDS inlet.

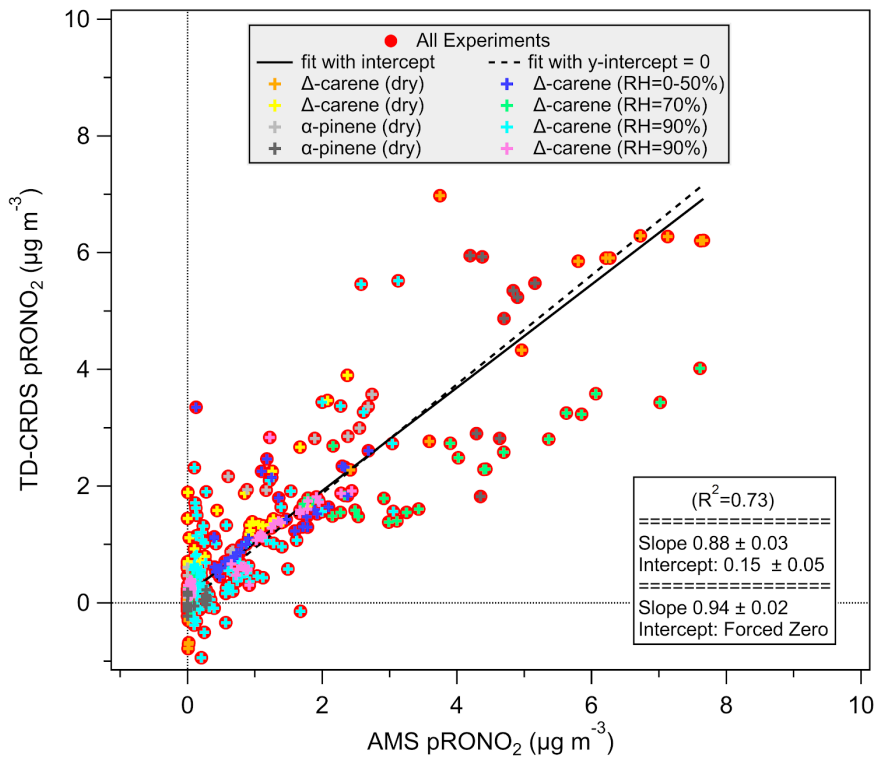


Figure 8. Background and denuder-breakthrough-corrected aerosol-phase ANs measured by the TD-CRDS, compared to the high-resolution AMS organic nitrate aerosol mass loading. Fits are orthogonal distance regression (ODR).

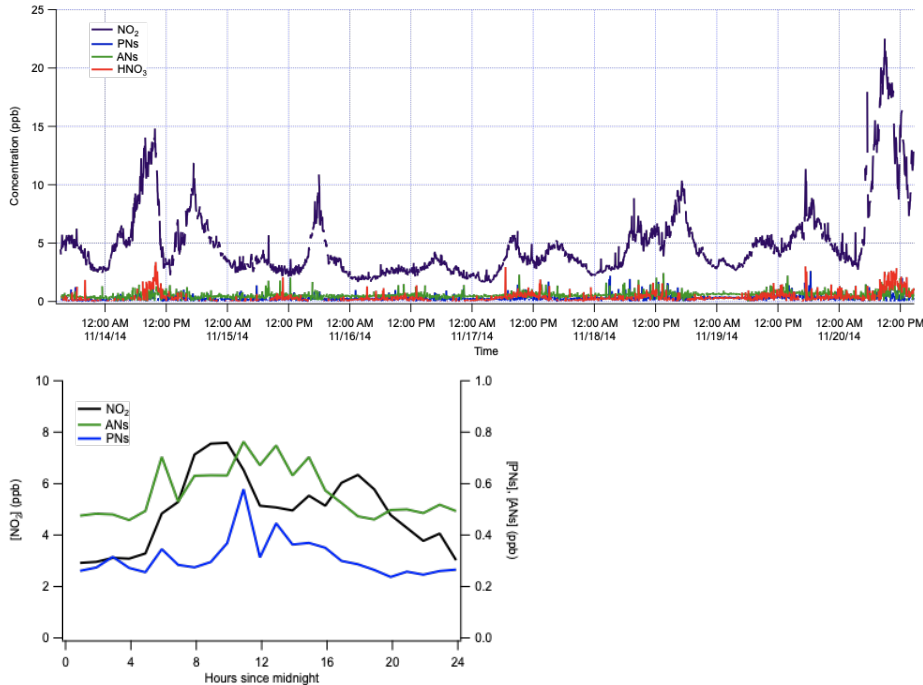
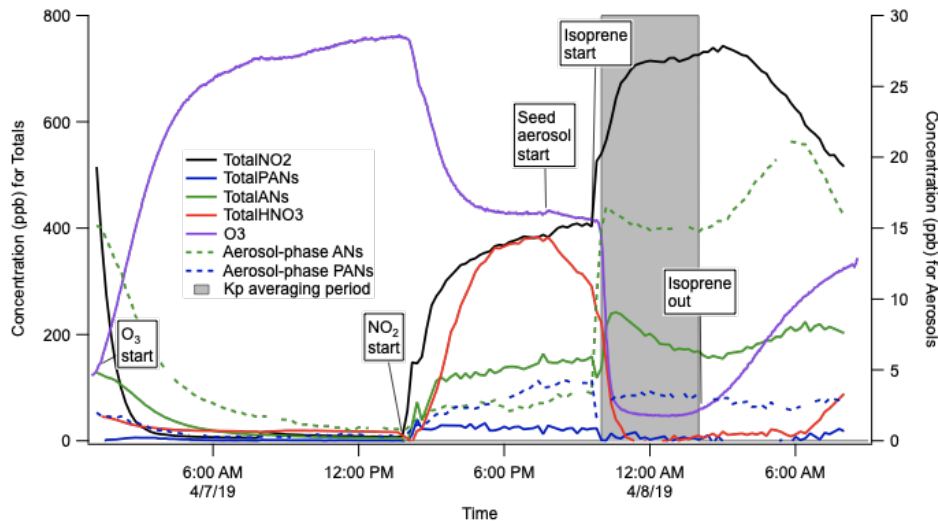


Figure 9. Representative measurements of NO₂, PN, AN, and HNO₃ concentrations from ambient air in November, 2014 in Portland OR. One week of data is shown to illustrate measurements of typical variability, alongside an average diurnal cycle from this period.

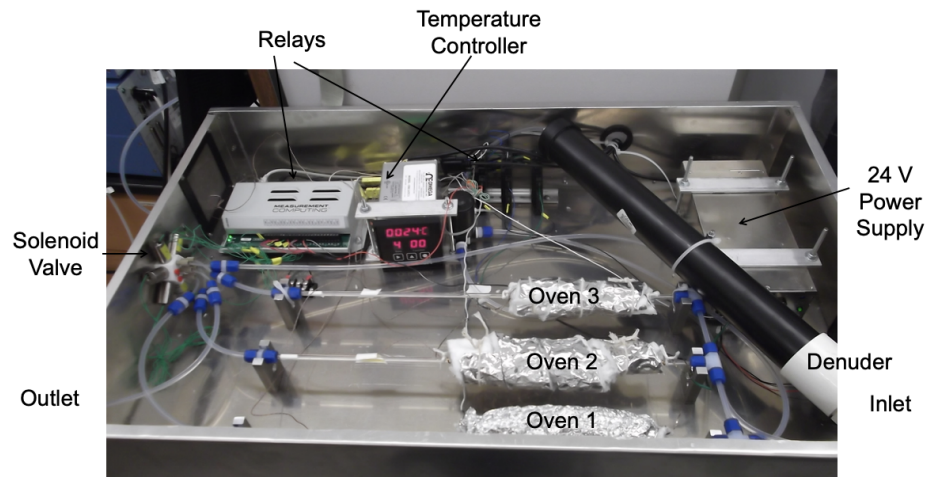


675

Figure 10. Example experiment to determine the bulk organonitrate partitioning (K_p) from $\text{NO}_3 +$ isoprene products in the Reed Environmental Chamber, at $20 \mu\text{g m}^{-3}$ ammonium sulfate background aerosol. Note that these traces are not corrected for N_2O_5 interferences in the ANs and PANs channel, but N_2O_5 was fully consumed in the period of K_p determination.

680

Supplemental Information



685 **Figure S1.** Oven inlet box.

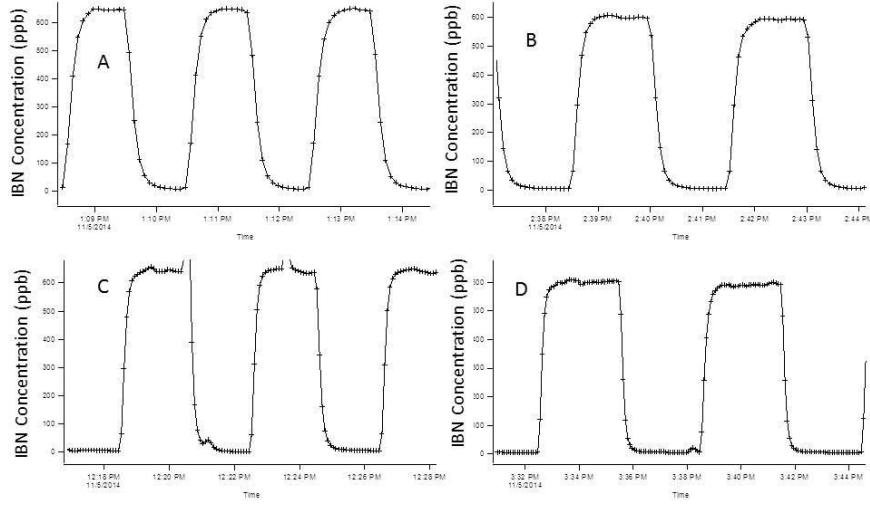


Figure S2. Channel switching frequency testing. Panel A shows 30 second sampling time, B 45 seconds, C 60 seconds, and D 90 seconds.

690

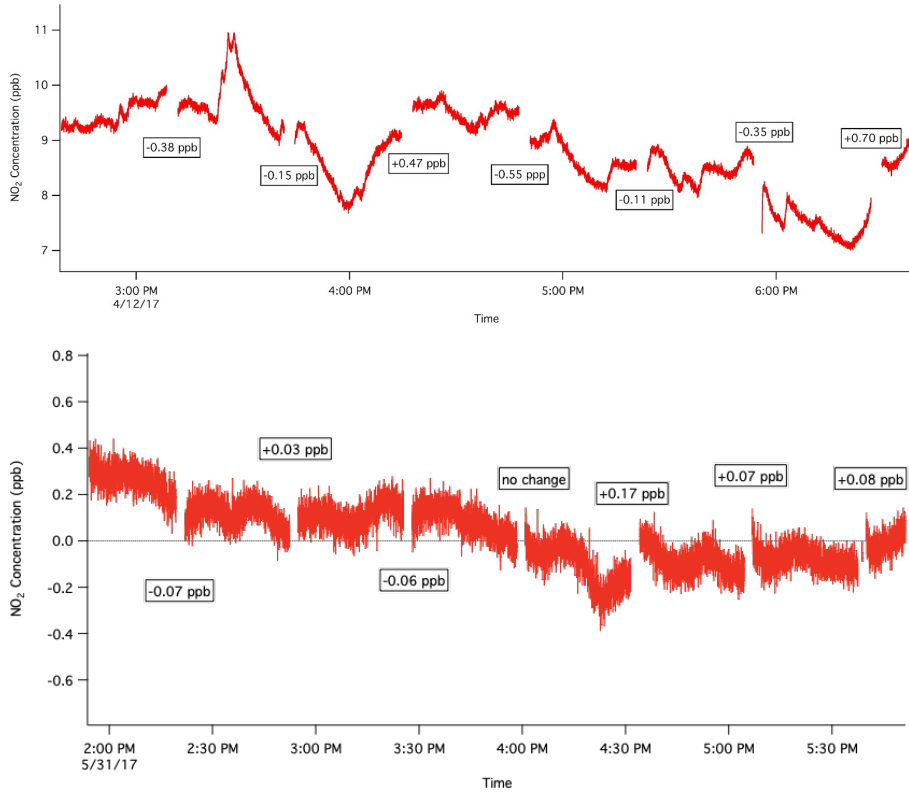


Figure S3. CRDS running for 4 hours on room air (upper panel) or zero air (lower panel). Seven instrument zeroes are visible across each timeseries to show the typical changes in signal. For the detection limit analysis included in the manuscript, the standard deviation of the zero signal measured over the full length of the lower panel was calculated, and found to be $\sigma_{\text{zero}} = 0.16 \text{ ppb}$.

Table S1. Rate constants for different species used in kinetics model.

Dissociation / Recombination Reactions	Dissociation rate parameters (Day et al., 2002, Table 1)				Recombination parameters ("JPL Data Evaluation" 2015, Table 2-1)			
	k_o^a	a^a	k_h^b	b^b	$k_o^{300,c}$	n^c	$k_o^{300,d}$	m^d
$PN \leftrightarrow NO_2 + CH_3C(O)OO$	4.9×10^{-3}	12100	4×10^{16}	13600	9.7×10^{-29}	5.6	9.3×10^{-12}	1.5
$AN \leftrightarrow NO_2 + C_2H_5CO$ or C_3H_7O	-	-	3.16×10^{16}	20129	2×10^{-27}	4	2.8×10^{-11}	1
$HNO_3 \leftrightarrow NO_2 + OH$	$(1.82 \times 10^{-4}) (T/298)^{-1.98}$	24004	2×10^{15}	24658	1.8×10^{-30}	3	2.8×10^{-11}	0
Loss Reaction	Rate constant							
$OH \rightarrow \text{walls}^e$	46 s^{-1}							
$n-C_4H_9O + O_2 \rightarrow \text{products}^f$	$(8.9 \times 10^{-14})(e^{-550/T}) \text{ cm}^3 \text{ molecule}^{-1} \text{ s}^{-1}$							

a. Low pressure limit $k_o(T) = k_o \exp(-a/T)$, where T is temperature in Kelvin, $\text{cm}^3 \text{ molecule}^{-1} \text{ s}^{-1}$
 b. High pressure limit $k_h(T) = k_h \exp(-b/T)$, where T is temperature in Kelvin, $\text{cm}^3 \text{ molecule}^{-1} \text{ s}^{-1}$
 c. Low pressure limit $k_o(T) = k_o^{300} (T/300)^{-n}$, where T is temperature in Kelvin, $\text{cm}^3 \text{ molecule}^{-1} \text{ s}^{-1}$
 d. High pressure limit $k_o(T) = k_o^{300} (T/300)^{-m}$, where T is temperature in Kelvin, $\text{cm}^3 \text{ molecule}^{-1} \text{ s}^{-1}$
 e. Knopf, Pöschl, and Shiraiwa 2015
 f. IUPAC evaluation, reaction RO_5, <http://iupac.pole-ether.fr/>

Deleted: 0

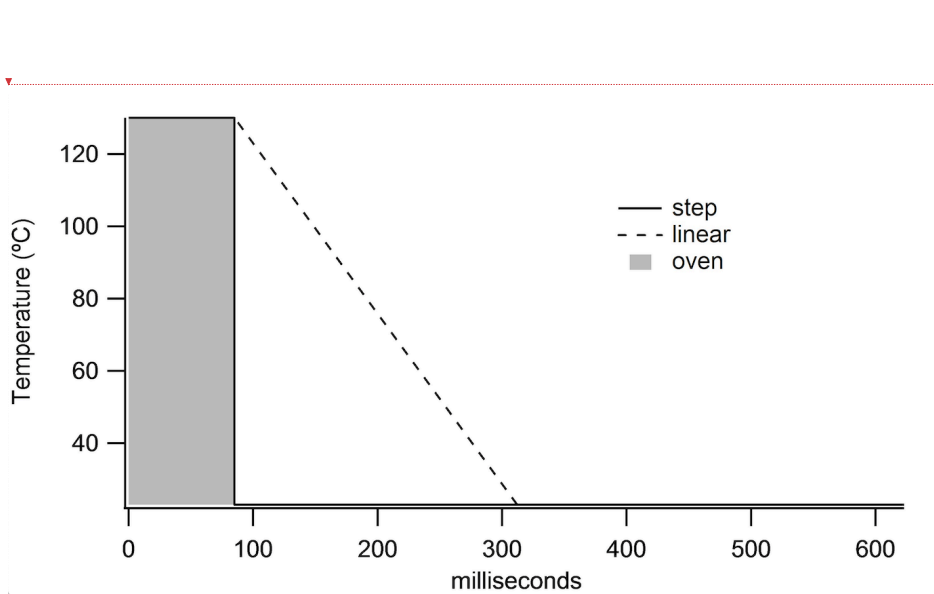
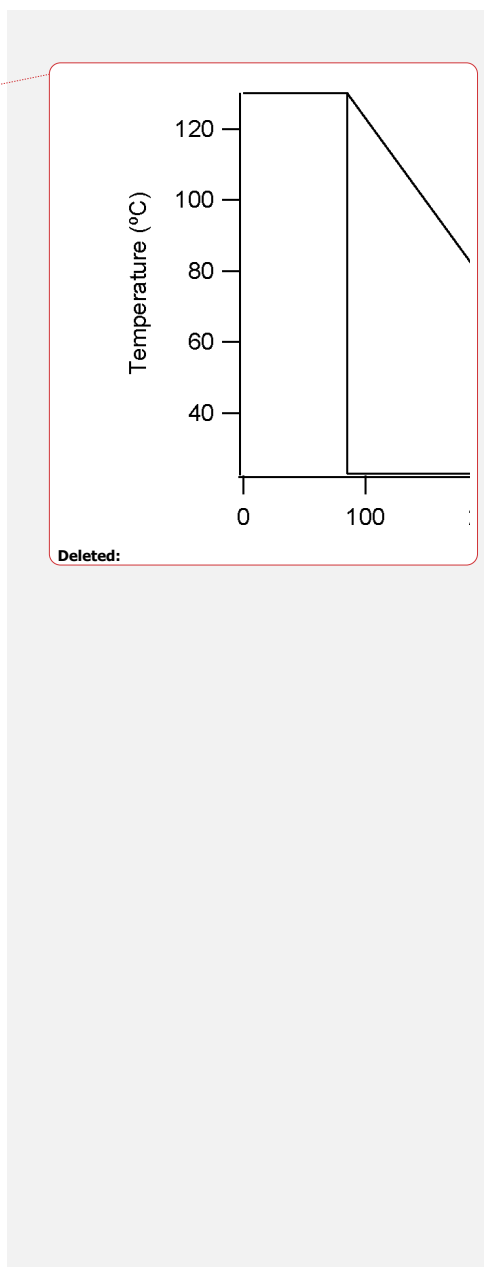


Figure S4. Two considered models of cooling rates in the quartz tubing after the PN oven.



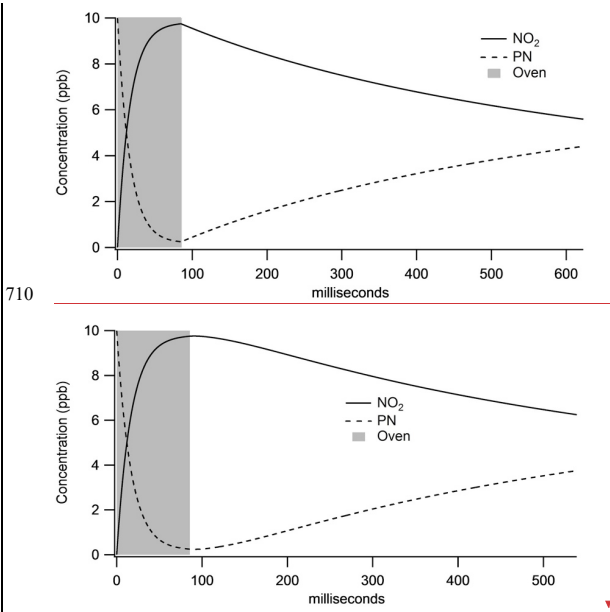
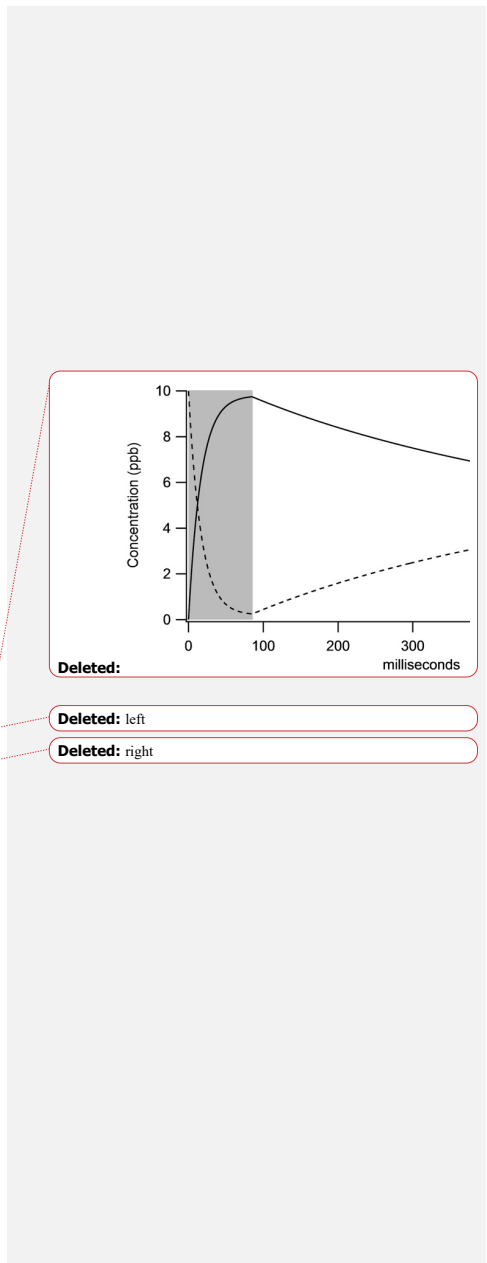


Figure S5. Model of PN dissociation through an oven at 120°C, using both step function (top) and linear temperature decay (bottom). Shaded region is the heated portion of the oven.



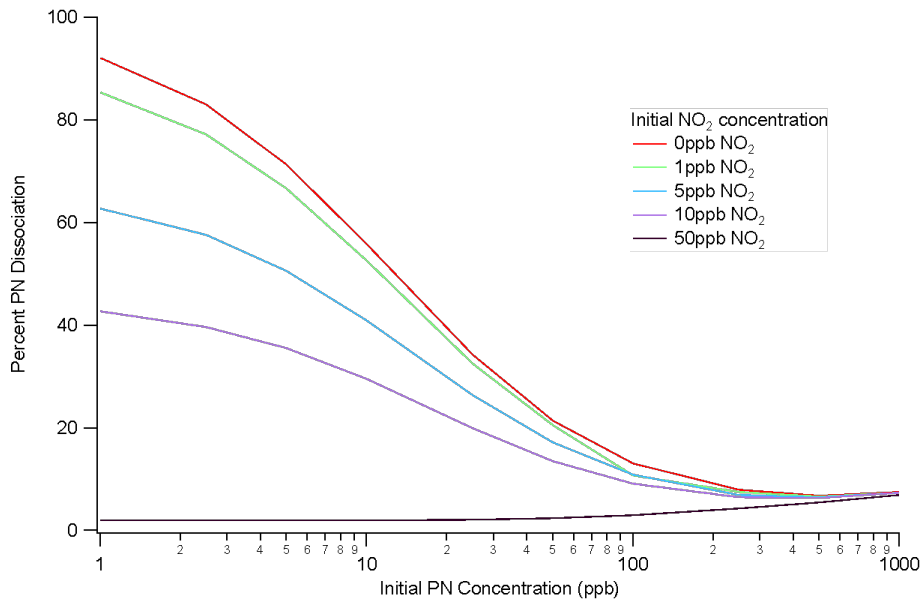
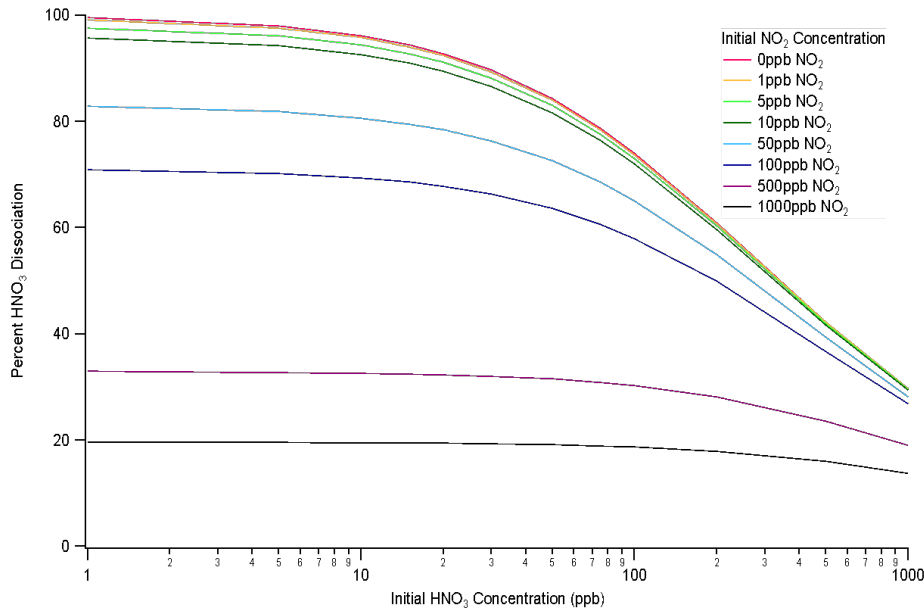
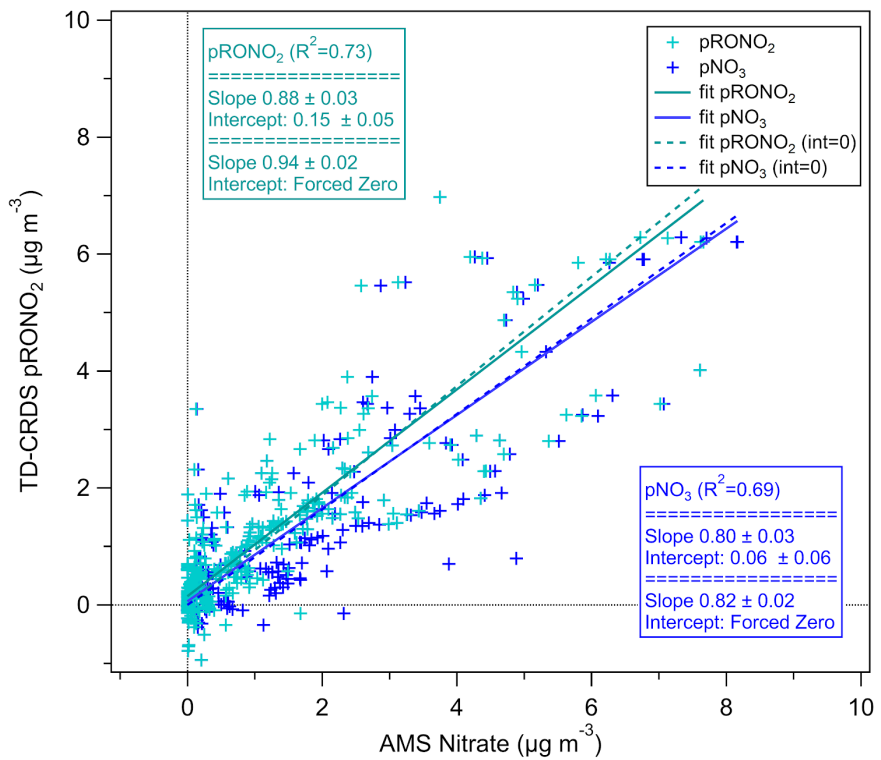


Figure S6. Percent PNs detected at CRDS at different initial concentrations of PNs and NO₂. Most work is done in the lower 720 concentration range of both PNs and NO₂, where the percent of PNs that remain dissociated to the detector is relatively higher; however we note the recombination effect here is larger than for ANs or HNO₃ (see Figure S7). Percent dissociated is equivalent to percent detected.



725 **Figure S7.** Percent HNO_3 detected at CRDS at different initial concentrations of nitric acid and NO_2 . Most work is done in the lower concentration range of both HNO_3 and NO_2 , where the percent HNO_3 that remains dissociated to the detector is high. Percent dissociated is equivalent to percent detected.



730 **Figure S8.** TD-CRDS organic nitrate vs AMS total nitrate (pNO₃) and apportioned organic nitrate fraction (pRONO₂).